PROCEEDINGS OF THE KECK GEOLOGY CONSORTIUM

Volume 38
2025-2026 Projects

Dr. Cameron Davidson and Dr. Karl Wirth, Editors
Co-Directors, Keck Geology Consortium

Theresa Klauer
Keck Geology Consortium Administrative Assistant
Macalester College

Keck Geology Consortium
Macalester College
1600 Grand Ave, St. Paul, MN 55105
(651) 696-6108, Info@KeckGeology.org

ISSN# 1528-7491
doi: 10.18277/AKRSG.2026.38

Funding Provided by:
Keck Geology Consortium Member Institutions
The National Science Foundation Grant NSF-REU 2050697

PROCEEDINGS OF THE KECK GEOLOGY CONSORTIUM

2025-2026 Projects

Cameron Davidson Editor and Co-Director Carleton College	Keck Geology Consortium Macalester College 1600 Grand Ave. St Paul, MN 55105	Karl Wirth Editor and Co-Director Macalester College

Keck Geology Consortium Member Institutions:

Amherst College, Beloit College, Carleton College, Colgate University, The College of Wooster, The Colorado College, Franklin & Marshall College, Macalester College, Pomona College, Trinity University, Washington & Lee University, Whitman College

2025-2026 GATEWAY PROJECTS

TRACE-METAL BEARING SULFIDES AND OXIDES IN CAMBRIAN STRATA OF WEST-CENTRAL WISCONSIN
Faculty: JAY ZAMBITO and JIM ROUGVIE, Beloit College
Peer Mentors: SIMONE DE MONTIGNY and LIA DIRKS, Beloit College
Students: DANIYAR ALI, Colgate University; MADELEINE DIESL, Mount Holyoke College; ANNABELLE DURBIN, Macalester College; ARIN GOLDSTEIN, Amherst College; SAMANTHA HUEPER, Penn State University; DONOVAN JENSEN, Univ Illinois-Urbana Champaign; ARAHAN LIM, Univ California-Berkeley; PARKER MARCHETTI, William & Mary; HALLIE STRAND, Columbia University; ZOE WEISSMAN, Hamilton College

ASSESSING PRE-ERUPTIVE CONTROLS ON EXPLOSIVE AND NON-EXPLOSIVE VOLCANIC ERUPTIONS
Faculty: KURT KNESEL, Trinity University
Peer Mentor: CHARLES LONG, Trinity University
Students: ELISA GARCIA, Franklin and Marshall College; WILLIAM HAMILTON, Trinity University; OWEN KALAPACA, Univ Texas-San Antonio; MATTHEW SANTOS, University of Houston; MORGAN TERPSTRA, Grand Valley State University

GEOLOGIC BOUNDARIES: IDENTIFYING THE TRANSITION TO THE ANTHROPOCENE IN LAKE WONONSCOPOMUC, CONNECTICUT
Faculty: DAVE JONES and ANNA MARTINI, Amherst College; TIM KU, Wesleyan University
Peer Mentor: MIA SANCHEZ, Amherst College
Students: LIAM CHAVEZ, Univ Texas-El Paso; ANTHONY COLLAZO, Univ Puerto Rico-Mayaguez; MOLLY GREANEY, Amherst College; RILEY HIGGINS, College of Wooster; DIVYANOOR KAUR, Rutgers University; JESSE LEBOLT, Amherst College; LILLIANNE MCCULLY, Beloit College; OSCAR SALAS ROMERO, Highline College; KATHRYN TESKE, Macalester College

2025-2026 ADVANCED PROJECTS

CLIMATE AND TREE GROWTH IN A TEMPERATE COASTAL RAINFOREST, SOUTHEAST ALASKA
Faculty: GREG WILES and NICK WIESENBERG, The College of Wooster
Students: LYNNSEY DELIO, The College of Wooster; ISABEL HELD, Scripps College; DEXTER PAKULA, Carleton College; LEV SUGERMAN-BROZAN, Colorado College; LANDON VAUGHAN, Trinity University

Conference Presentations – Wisconsin Gateway Project

Ali, D., Weissman, Z., Rougvie, J., and Zambito, J., 2025, Magnetic Susceptibility Stratigraphy of the Cambrian Lone Rock Formation, Wisconsin, U.S.A., *in* Geological Society of America Abstracts with Programs, v. 57, p. 2025AM – 10677, doi:10.1130/abs/2025AM-10677.

De Montigny, S., Diesl, M., Goldstein, A., Hueper, S., Rougvie, J., and Zambito, J., 2025, Trace-Metal Bearing Sulfides and Oxides Constrain Mississippi Valley Type Mineralization in the Cambrian St. Lawrence Formation, Western Wisconsin, *in* Geological Society of America Abstracts with Programs, p. 2025AM – 10701, doi:10.1130/abs/2025AM-10701.

Dirks, L., Jensen, D., Marchetti, P., Rougvie, J., and Zambito, J., 2025, New Implications for Paleoenvironmental Reconstruction of the Eau Claire Formation in its Type Area, *in* Geological Society of America Abstracts with Programs, p. 2025AM – 10724, doi:10.1130/abs/2025AM-10724.

Durbin, A., Lim, A., Strand, H., Rougvie, J., and Zambito, J., 2025, Trace Metal Geochemistry and Mineralogy of Diagenesis in the Cambrian Jordan Formation, Western Wisconsin, *in* Geological Society of America Abstracts with Programs, p. 2025AM – 10755, doi:10.1130/abs/2025AM-10755.

Conference Presentations – Connecticut Gateway Project

Greaney, M., Kaur, D., Chavez, L., Lebolt, J., Collazo, A., Higgins, R., Jones, D.S., Martini, A.M., Ku, T.C.W., Teske, K., McCully, L., Salas Romero, O., and Sanchez, M., 2025, Reconstructing Anthropogenic Activity Using Elemental Proxies in Sediment Cores from Lake Wononscopomuc, CT, Abstract PP51E-0414 presented at AGU25, 15-19 Dec.

Lebolt, J., Teske, K., McCully, L., Salas Romero, O., Greaney, M., Kaur, D., Higgins, R., Collazo, A., Chavez, L., Sanchez, M., Jones, D.S., Martini, A.M., Ku, T.C.W., and Oostenink, C., 2025, A ^{210}Pb-based Age Model and Hg Record of Industrial Impact from Lake Wononscopomuc, CT, Abstract PP51E-0412 presented at AGU25, 15-19 Dec.

Conference Presentations – Texas Gateway Project

Long, C., Gingerich, M., Hamilton, W., Kalapaca, O., Santos, M., Terpstra, M., and Knesel, K., 2025, Investigating the Effect of Nanolitization on Melt Viscosity using Raman Spectroscopy, *in* Abstracts with Programs - Geological Society of America, v. 57, p. 2025AM – 11234, doi:10.1130/abs/2025AM-11234.

Santos, M., Kalapaca, O., Long, C., Gingerich, M., and Knesel, K., 2025, Modeling the Viscosity of Flow-banded Rhyolite using Raman Spectroscopy, *in* Abstracts with Programs - Geological Society of America, v. 57, p. 2025AM – 11212, doi:10.1130/abs/2025AM-11212.

Terpstra, M., Hamilton, W., Long, C., Gingerich, M., and Knesel, K., 2025, Nano-scale Characterization of Rhyolite Lava using Raman Microscopy, *in* Abstracts with Programs - Geological Society of America, v. 57, p. 2025AM – 10288, doi:10.1130/abs/2025AM-10288.

Conference Presentations – Alaska Advanced Project

Delio, L., Wiles, G.C., and Wiesenberg, N., 2025, Using alaskan tree-rings to reconstruct lake michigan-huron levels, *in* Abstracts with Programs - Geological Society of America, Geological Society of America (GSA), v. 57, p. Abstract no. 106-29, doi:10.1130/abs/2025AM-6966.

Held, I., Wiles, G., and Gaines, R., 2025, Analysis of monthly mendenhall river discharge and possible tree-ring based reconstruction, *in* Abstracts with Programs - Geological Society of America, Geological Society of America (GSA), v. 57, p. Abstract no. 106-32, doi:10.1130/abs/2025AM-6978.

Pakula, D.C., Wiles, G.C., and Wiesenberg, N., 2025, Investigating tree-ring evidence for an indian ocean-gulf of Alaska teleconnection, *in* Abstracts with Programs - Geological Society of America, Geological Society of America (GSA), v. 57, p. Abstract no. 106-30, doi:10.1130/abs/2025AM-6988.

Sugerman-Brozan, L., Lawman, A., and Wiles, G., 2025, Investigating volcanically forced shifts in North Pacific climate in model simulations and Alaska tree ring records, *in* Abstracts with Programs - Geological Society of America, Geological Society of America (GSA), v. 57, p. Abstract no. 106-33, doi:10.1130/abs/2025AM-6983.

Vaughan, L., Wiles, G.C., and Wiesenberg, N., 2025, A protracted winter: tree-rings indicate an abrupt and persistent cooling in 1698 and 1699 Ce, Gulf of Alaska, *in* Abstracts with Programs - Geological Society of America, Geological Society of America (GSA), v. 57, p. Abstract no. 106-5, doi:10.1130/abs/2025AM-6970.

Short Contributions – Alaska Advanced Project

KECK Geology Consortium
Learning Science Through Research
Published by the Keck Geology Consortium
Short Contributions
Keck Geology Consortium
Volume 38
May 2026
doi: 10.18277/AKRSG.2026.38.01

KECK SEAK25 - CLIMATE AND TREE GROWTH IN A TEMPERATE COASTAL RAINFOREST, SOUTHEAST ALASKA

GREG WILES and NICK WIESENBERG, The College of Wooster

INTRODUCTION

The State of the Global Climate report of the World Meteorological Organization (WMO, 2026) highlights the continued warming of the planet in the air and oceans, the Earth's energy imbalance, and a looming strong El Niño that will likely exacerbate warming in 2026-2027. North Pacific coastal forests provide a long-term record of these ongoing thermal changes and allow us to explore how linkages, teleconnections and abrupt events impact warming.

Tree-rings are exactly calendar-dated records of environmental change, and in southern Alaska, trees are primarily sensitive to temperature variations. Previous studies have utilized tree-ring records to reconstruct local and hemispheric temperatures (Wiles et al., 2014, 2026; Wilson et al, 2016, 2017; Anchukaitis et al., 2017), glacier mass balance (Malcomb and Wiles, 2013), and hydroclimate in North America (Wiles et al., 2023).This project aimed to continue developing and analyzing new tree-ring chronologies adding to a growing network of records from Alaska and the Yukon (Fig. 1). Keck-SEAK25 student projects have expanded the scope of this work using the newly collected and previous tree-ring records in climate analyses and modeling investigations.

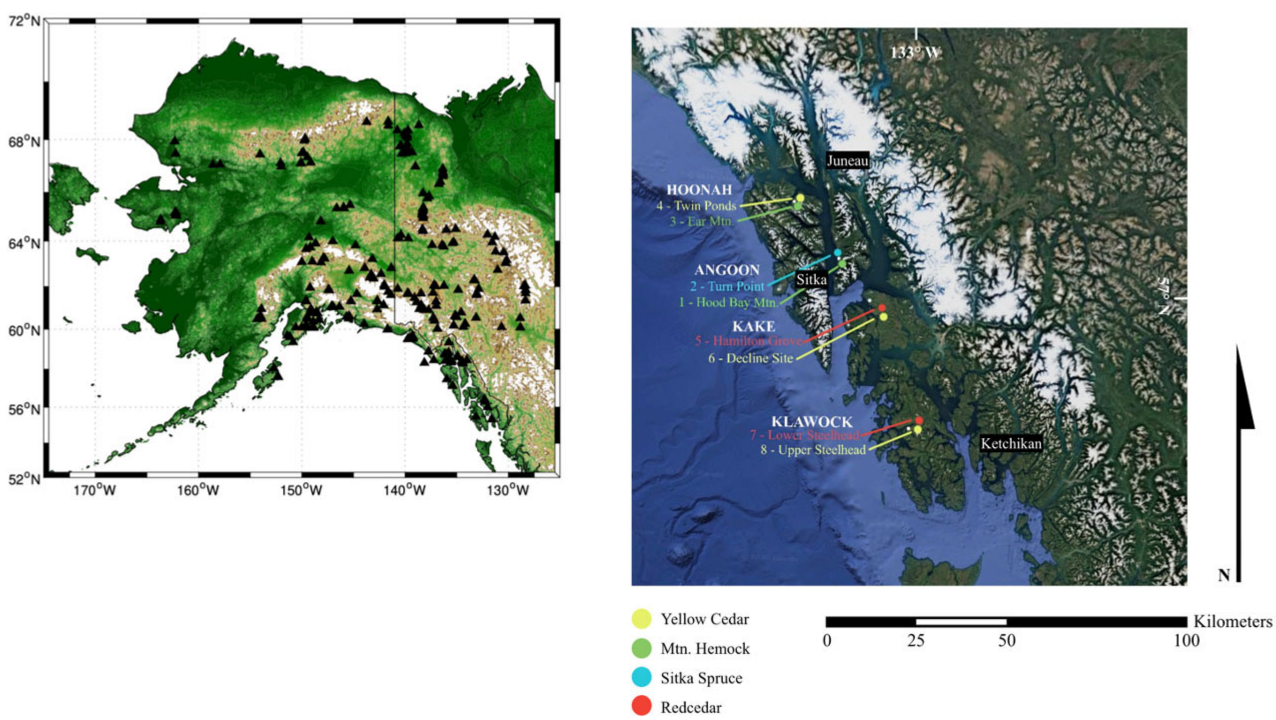

Figure 1. Tree-ring chronologies from Alaska and the Yukon: This project added to this dataset and used the larger network (left map; (E.R. Cook, pers. comm.) for climate reconstruction and modeling. The detail map (right) are the locations of 8 tree-ring width chronologies developed with AYS collaboration over the past 5 years and recently contributed to the ITRDB. Those at Angoon, the Turn Point and Hood Bay Mtn. sites were generated as part of this SEAK25 project.

Another aspect of the project leveraged The Wooster Tree Ring Lab's (WTRL) collaboration with the Alaska Youth Stewards (AYS), which together over the past five years has been actively investigating new tree-ring sites in the forests of Southeast Alaska (SEAK). AYS serve the Tlingit-Haida community in SEAK preparing youth for environmentally-related careers and college. Our collaboration began in 2020 and has grown to include communities in Hoonah, Angoon, Kake and Klawock, which are Tlingit villages in SEAK. Three of these villages, Kake, Hoonah and Klawock, were visited in the summers of 2022 through 2024, and Angoon was the destination of the 2025 field season described here. The aim of this collaboration is to work in the field with the AYS groups, visiting tree-ring sites that the groups have discovered and sampling Sitka spruce, red and yellow cedar, and mountain hemlock stands. The summer 2025 work in Angoon centered on Sitka spruce and mountain hemlock sites. From these collections and those of previous years, we assembled ring-width, tree-ring data, analyzed them for their climate significance, and connected the tree-ring data to climate, forest health, and their potential as a record of past indigenous use, such as bark stripping manifested as culturally modified trees (CMTs; McGrath et al., 2014).

The SEAK25 research group first worked in the Wooster Tree Ring Lab in Ohio learning the fundamentals of tree-ring sampling and lab analyses. The group developed a redcedar tree-ring record from SEAK sampled in previous years. Subsequently, we travelled to Juneau and then Angoon working with the AYS team lead by Gabrielle Sjoberg and Eric Benedict. After tree-ring collections and collaboration in Alaska, the team returned to Wooster to develop the tree-ring records and to conduct the analyses for their individual projects. Projects examined chronologies in the tree-ring archive and newly-produced records to model climate indices and hydroclimate variables and to explore the role of volcanic forcing in North Pacific climate. Several results and research questions not addressed by the student projects emerged during our summer analyses, which we will outline in the results section, followed by a description of each student's project.

RESULTS

Collectively the group developed and analyzed a redcedar ring-width series for its climate signal and then contributed the tree-ring data to the International Tree Ring Data Bank (ITRDB). This Hamilton Grove site is the first redcedar contribution from Alaska (Fig. 2), which was previously collected in Kake, Alaska (Fig. 1). Twenty-four tree cores from the Hamilton Grove site were cross-dated and assembled into a tree-ring ring-width chronology (Fig. 2). We compared this chronology with 150 years of monthly climate records from Sitka, Alaska to determine the climate response in the ring-widths. This statistical comparison yields a correlation (r) that can be assessed for significance using a p-value and the sample size, which is the number of years that the tree-ring record overlaps with the monthly climate records. There is a clear redcedar climate signal and strong signficant correlation with winter temperature ($r = 0.38$; $p < 0.00001$), which is an average of January through March. This is an unexpected result as most trees along the Gulf of Alaska respond to summer temperature changes (Wiles et al., 2014). The 1876 ring is the most narrow in the record and corresponds with a strong El Niño and one of most profound droughts and famines in other parts of the world (Fig. 2; Singh et al., 2018). The relationship between the Gulf of Alaska winter cooling and this strong El Niño event is uncertain.

Sampling of Sitka spruce at Angoon (the Turn Point site) has resulted in a tree-ring width series from low elevation tree-ring series (Fig. 3) combining two sampling sites. The trees included samples from Culturally Modified Trees (CMTs) that were utilized in the past for harvesting sap used as fire-starter.

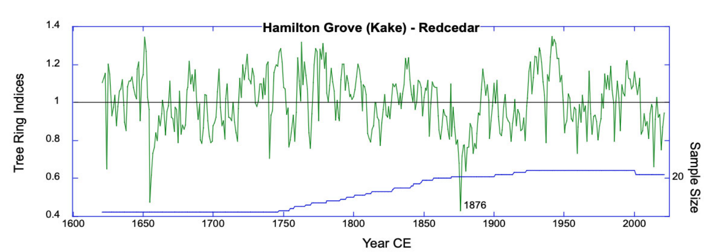

Figure 2. The Hamilton Grove chronology from Kake western redcedar. This redcedar chronology is the first for Alaska and was sampled at the northernmost redcedar site. Other sites further north have been reported, but are not confirmed (pers. comm. B. Buma). The climate signal here is a strong positive relationship with winter temperatures.

This Turn Point tree-ring series has a strong positive relationship with Sitka (January – May average; r = 0.45, p < 0.00001; N = 85) minimum temperatures (nighttime temperatures).

The Angoon spruce site (Fig. 3a) is a low elevation site and the relationship with minimum temperatures is unsteady through time (Fig. 3b). Correlations prior to 1976 are strong with gridded temperature records. However, after 1976, there is virtually no relationship (Fig. 3b). The reason for this change is uncertain but, may be related to the well-known shift in North Pacific climate in 1976-77 (Ebbysmeyer, 1991).

The other site from Angoon, Mountain Hemlock, was sampled in summer 2025 on Hood Bay Mountain (Fig. 4). This site was sampled near treeline and has the strongest relationship with minimum June-August temperatures from Sitka (N=87; r = 0.37; p < 0.0004). The low growth intervals in the chronology (Fig. 4a) are consistent with the 1809 volcanic cooling (Leland et al., 2023) and the cooling around 1698 CE. The apparent drop off in growth after about 1975, which may have occurred after a disturbance at the site, is worth further investigation.

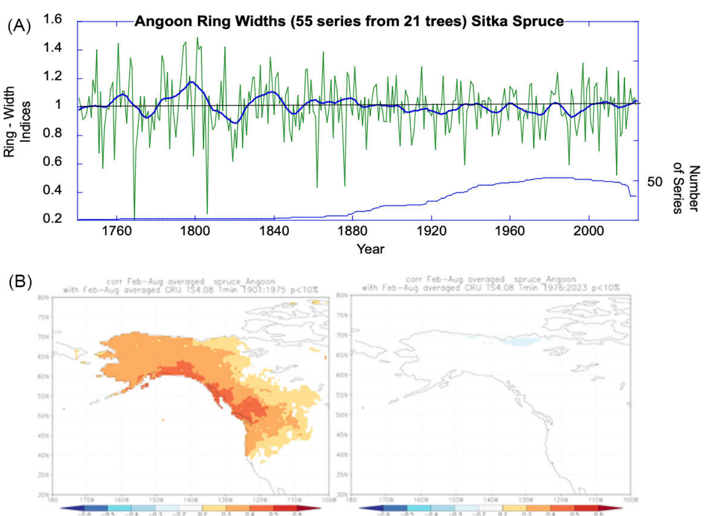

Figure 3. A) Angoon Sitka spruce site. The chronology is well-replicated for the past 150 years and consists of spruce trees at Angoon and at the Turn Point site across the strait from the town. B) Left panel: Prior to 1975 there is a strong positive relationship with minimum temperatures and spruce tree growth. Right panel: after 1975 there is virtually no relationship, which may suggest warming is no longer beneficial to spruce growth or temperature is not limiting the growth of spruce after 1975.

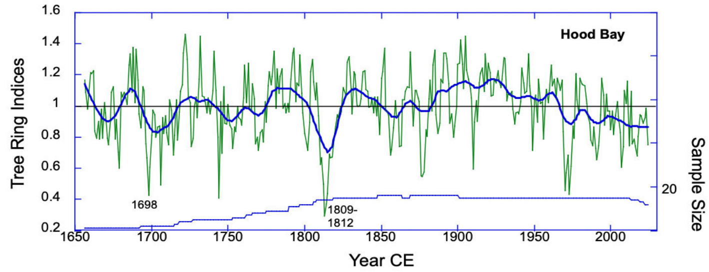

Figure 4. The Hood Bay Mountain, mountain hemlock ring-width chronology. This series is a record of June-August temperatures and shows the volcanic cooling associated with volcanic eruptions at 1698 and 1809. Note also the drop-off after the mid-1970s.

STUDENT PROJECTS

Lynnsey Delio (The College of Wooster) Leveraging the Pacific North America (PNA) teleconnection, Lynnsey Delio used a network of six ring-width series from Southeast Alaska to model the variability of the lake Michigan-Huron Great Lake system, reconstructing the observational record back to 1600 CE. Delio identified several high lake levels that appear to be linked to large-scale volcanic events perhaps due to decreased evaporation with increased ice cover during volcanically-forced coolings.

Isabel Held (Scripps College) In Juneau the group updated the Mendenhall Trail tree-ring series originally sampled in 1999. Isabel Held linked the tree growth in the Juneau region to the USGS gaging station at the Mendenhall River exploring the possibility of reconstructing this river flow. This work is particularly relevant as the 13 August 2025 glacial outburst flood (GLOF) on the Mendenhall River was the largest on record and previous GLOFs have resulted in considerable loss of property.

Dexter Pakula (Carleton College) The group collectively developed the first redcedar tree-ring chronology from Alaska that was formerly sampled from Kake Alaska by The College of Wooster faculty and staff and the Alaska Youth Stewards. The climate analysis of this series was surprisingly strongly correlated with winter temperatures, potentially yielding a proxy for cold-season temperature change. Significantly, this redcedar record showed the most-narrow ring (1876 CE), which corresponds with a major El Niño event. This connection served as a catalyst for Dexter Pakula to investigate and develop the linkages between the monsoonal indices from

Southeast Asia and the North Pacific.

Lev Sugerman-Brozan (Colorado College) examined the volcanic forcing of decadal climate in the North Pacific using a comparison between the observational (based on tree rings) record and a Community Earth System Model Last Millenium Ensemble (CESM-LME) model. He examined the 1452, 1697-98 and 1809 events and their influence on forcing persistent cooling in the North Pacific.

Landon Vaughan (Trinity University) Focusing on the late 1690s in Alaska Yellow Cedar, Landon Vaughn determined that the most-narrow rings in the past several centuries in SEAK were the 1698-99 rings, which are likely associated with the “winter following winter” as reported in the oral histories of the Tlingit. This crucial event was likely volcanically-forced and occurred at the same time the large glacier in Glacier Bay was advancing, leading to the eviction of the Tlingit from their native homeland. The late 1600s was an interval comment to all five of the studies and the relationship between the role of volcanic cooling, natural changes in climate along with solar forcing during this phase of the Little Ice Age is a source of ongoing discussion.

The SEAK25 team all presented their results at the National Meeting of the Geological Society of America at San Antonio, TX. Our SEAK25 work in Angoon marked the 5th year of collaboration between the AYS group and The Wooster Tree Ring Lab. The relevance of the results summarized here and in the student project descriptions is underscored by the new (2026) report of the WMO and observations linking the ongoing Earth’s energy imbalance, the looming strong El Niño event that is likely to continue into 2026-27, and the response of the North Pacific ocean air-sea temperatures.

ACKNOWLEDGEMENTS

This material is based upon work supported by the Keck Geology Consortium and the National Science Foundation (NSF) under Grant No. 2050697 and prior work with AYS was supported by NSF grants P2C2-2002561and P2C2-2002454. We also thank The College of Wooster Danner Fund for financial support. We are grateful to the Angoon 2025 AYS participants for an enjoyable and productive time in Alaska. S’eiltin Jamiann Hasselquist lead our groups in restoring gravesites in Angoon, while providing us with a memorable several days learning about the Tlingit-Haida history of the region.

REFERENCES

Anchukaitis, K.J., R. Wilson, K. Briffa, U. Büntgen, E.R. Cook, R.D. D’Arrigo, N. Davi, J. Esper, D. Frank, B. Gunnarson, G. Hegerl, S. Helama, S. Klesse, P.J. Krusic, H. Linderholm, V. Myglan, T. J. Osborn, Z. Peng, M. Rydval, L. Schneider, A. Schurer, G. Wiles and E. Zorita, 2017, Last millennium Northern Hemisphere summer temperatures from tree rings: Part II: spatially resolved reconstructions, Quaternary Science Reviews 134: 1-18, JQSR-D-16-00439R1.

Ebbesmeyer, C. C., D. R. Cayan, D. R. McLain, F. H. Nichols, D. H. Peterson, K. T. Redmond, 1991. 1976 step in the Pacific climate: Forty environmental changes between 1968–1975 and 1977–1985. Proc. Seventh Annual Pacific Climate Workshop, Asilomar, CA, California Dept. of Water Research, 115-126.

Leland, C., D’Arrigo, R., Davi, N., Anchukaitis, K. J., Andreu-Hayles, L., Porter, T. J., et al. (2023). A spatiotemporal assessment of extreme cold in northwestern North America following the unidentified 1809 CE volcanic eruption. Paleoceanography and Paleoclimatology, 38, e2022PA004581. https://doi.org/10.1029/2022PA004581.

Malcomb, N.L. and Wiles, G.C., 2013, Tree-ring based reconstructions of North American glacier mass balance through the Little Ice Age. Quaternary Research, http://dx.doi.org/10.1016/j.yqres.2012.11.005.

McGrath, S., Howell, W., Wiesenberg, N., Mennett, C., and Wiles, G., 2014, Three hundred years of continuity: a yellow cedar bark stripping site on Pleasant Island, Icy Strait, Southeast Alaska: Geological Society of America Abstracts with Programs. Vol. 46, No. 6, p. 247.

Singh, D., R. Seager, B. I. Cook, M. Cane, M. Ting, E. Cook, and M. Davis, 2018. Climate and the Global Famine of 1876–78. J. Climate, 31, 9445–9467, https://doi.org/10.1175/JCLI-D-18-0159.1.

Wendler, G., Galloway, K., and Stuefer, M., 2016. On the climate and climate change of Sitka, Southeast Alaska. Theor. Appl. Climatol. 126, 27–34. doi: 10. 1007/s00704- 015- 1542- 7.

Wiles, G.C., D'Arrigo, R.D., Barclay, D., Wilson, Jarvis, S. K., Vargo, L., Frank, D., 2014, Surface air temperature variability for the Gulf of Alaska over the past 1200 years: The Holocene, DOI: 10.1177/0959683613516815.

Wiles, G.C., Devereux, K., Gaglioti, B.V., D'Arrigo, R.D., 2023, A 420-Year Perspective on Winter Lake Erie Levels: Geophysical Research Letters 50 (1), doi.org/10.1029/2022GL099911.

Wiles, G., Wiesenberg, N., Lyon, E. , Young, N., Gaglioti, B. , Barclay, D., Cook, E.R., D'Arrigo, R. , Lawson, D., Mann, D., Wilson, R., Reid, E. , Davi, N., Frank, D., Panyushkina, I., Jull, A.J.T., and Howell, W., 2026. A 3870-Year Tree Ring Series for Climate Reconstruction and Dating from Southern Alaska: Arctic Workshop Abstract (Buffalo March 2026).

Wilson, R., D'Arrigo, R., Andreu-Hayles, L., Oelkers, R., Wiles, G., Anchukaitis, K and Davi, N., 2017, Blue Intensity based experiments for reconstructing North Pacific temperatures along the Gulf of Alaska: Clim. Past Discuss., doi:10.5194/cp-2017-26.

Wilson, R., Anchukaitis, K., Briffa, K., Büntgen, U., Cook, E., D' Arrigo, R., Davi, N., Esper, J., Frank, D Gunnarson, B., Hegerl, G., Helama, S., Klesse, S., Krusic, P., Linderholm, H.,

Myglan, V., Osborn, T., Rydval, M., Schneider, L., Schurer, A., Wiles, G., Zhang, P. and Zorita, E., 2016, Last millennium Northern Hemisphere summer temperatures from tree rings: Part I: the long-term context: Quaternary Science Reviews (2016), pp. 1-18 DOI information: 10.1016/j.quascirev.2015.12.005.

World Meteorological Organization (WMO). 2026, State of the Global Climate 2025. Geneva: WMO. https://wmo.int/publication-series/state-of-global-climate/state-of-global-climate-2025.

Learning Science Through Research
Published by the Keck Geology Consortium

Short Contributions
Keck Geology Consortium
Volume 38
May 2026
doi: 10.18277/AKRSG.2026.38.02

USING TREE RINGS FROM SOUTHEAST ALASKA TO RECONSTRUCT JANUARY – JUNE MICHIGAN-HURON LAKE LEVELS

LYNNSEY DELIO, The College of Wooster
Project Advisor: Greg Wiles

INTRODUCTION

The Great Lakes (GL) are the largest freshwater system on Earth, holding 84% of North America's water supply (EPA, 2025). People rely on the GL for drinking water, jobs in tourism, recreation, and marine transportation (NOAA, 2026), and they are home to more than 3,500 plant and animal species, some of which are found nowhere else on Earth (GLC, 2026). With over 7,250 kilometers of coastline in the U.S. (NOAA, 2026), flooding and coastal storm damage due to rising and falling lake levels is of primary concern (Meadows et al., 1997).

The objective of this study is to reconstruct historical lake levels in Lake Michigan-Huron (MH) leveraging the strong correlations between Alaskan tree ring series and monthly lake levels. Tree rings represent one year of a tree's life, making them a good indicator of annual climate variations. The main tree ring proxy used for climate reconstruction is tree ring width (TRW), which is influenced by changes in climate conditions (Popa et al., 2022). Favorable climate conditions result in strong tree growth, while extreme temperatures, precipitation, or other stress- inducing events may limit tree growth (Popa et al., 2022).

Teleconnections such as the Pacific North American teleconnection (PNA) provide the basis for the correlations and a context for the climatic similarities between these two geographically distinct regions. The PNA is a pattern of air pressure anomalies over the Pacific Ocean and North America that correlate with temperature and precipitation anomalies across North America (Dahlman, 2009). Rodionov (1994), Ghanbari and Bravo (2008), and Rogers and Coleman (2009) found that a negative PNA is linked to increased winter precipitation over the GL region (Fig. 1), possibly leading to higher lake levels. Furthermore, the PNA is correlated with atmospheric pressure all over the globe, and the GL region and Southeast Alaska have similar correlations (Fig. 2), indicating a teleconnection between the two areas.

This tree ring reconstruction will bridge the gap between geologic and observational records, linking historical and geologic lake level variability with tree rings and other observed climate conditions. Quinn and Sellinger (2006), and Wiles et al. (2023) have successfully used tree rings to reconstruct historical GL levels, whereas Brinkmann (1992) used tree rings

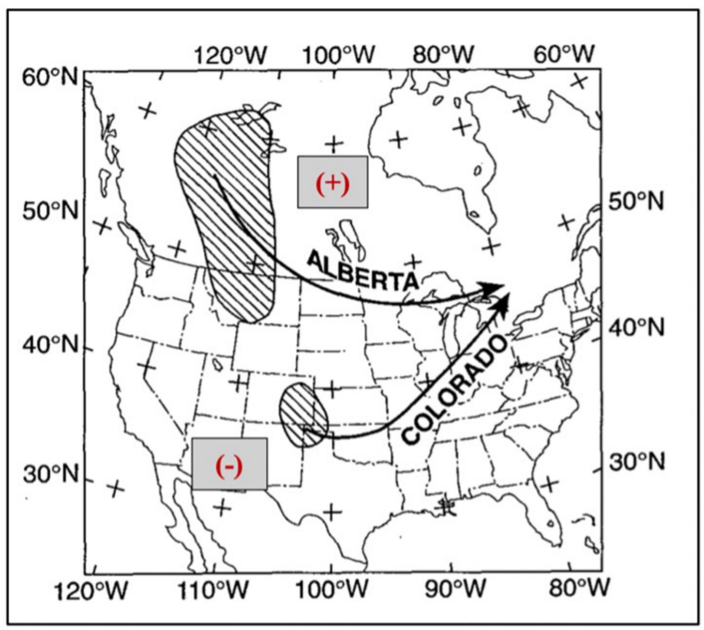

Figure 1. Cyclone activity and storm tracks during positive and negative PNA phases. Precipitation comes from Alberta during the positive phase, and Colorado during the negative phase, carrying significantly more precipitation during the negative because of proximity to the Gulf of Mexico and cyclogenesis east of the Rocky Mountains (Rodionov, 1994).

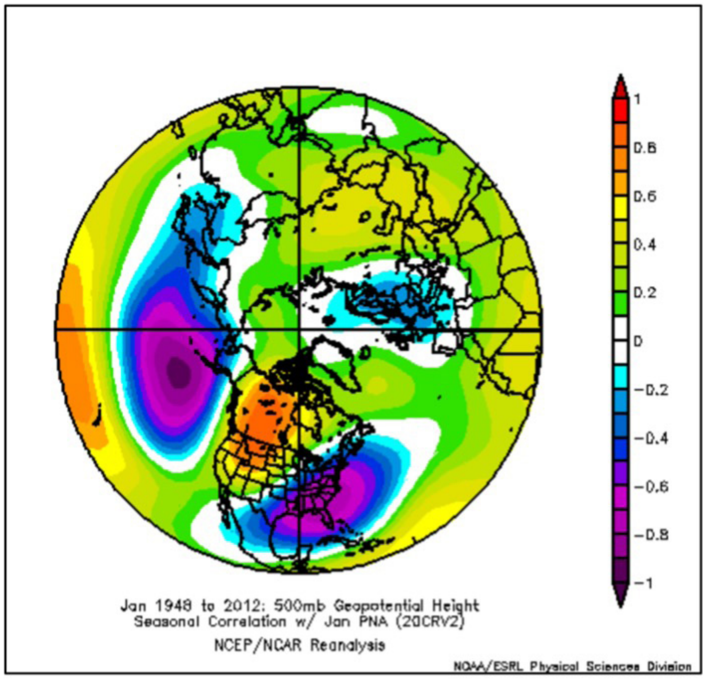

Figure 2. PNA correlated with atmospheric pressure. Monthly data from January 1948-2012 500mb heights, or the elevation above sea level where the atmospheric pressure is 500 millibars, correlated with the PNA index. Note the similar correlation between Southeast Alaska and the GL Region (NOAA, 2012).

to model GL net basin supply (NBS). Understanding historical peaks and lows in the lake level record will provide a basis for better anticipating lake level behavior in the present and into the future.

MATERIALS AND METHODS

Two hundred and two ring width chronologies were screened as potential predictors for lake level reconstruction (NOAA, 2026). These tree ring chronologies were standardized using the signal-free, age-dependent spline approach (Melvin & Briffa, 2008, 2014). This study uses the TRW of 10 chronologies from Southeast Alaska, significantly correlated at the 0.01 confidence level, the oldest tree reaching back to 1247 CE. The chronologies were then used to build a reconstruction of MH (Fig. 3) using a 2-PC model of PCReg (principal component regression analysis; Cook, E.R., 1985).

The reconstruction of Lake MH spans from 1650 to 1990 and has a calibration period of 131 years (1860 – 1990). Analysis of the tree ring chronologies and lake levels yielded a viable long season for reconstruction (January – June) as these months exhibited the strongest correlations between tree rings and lake

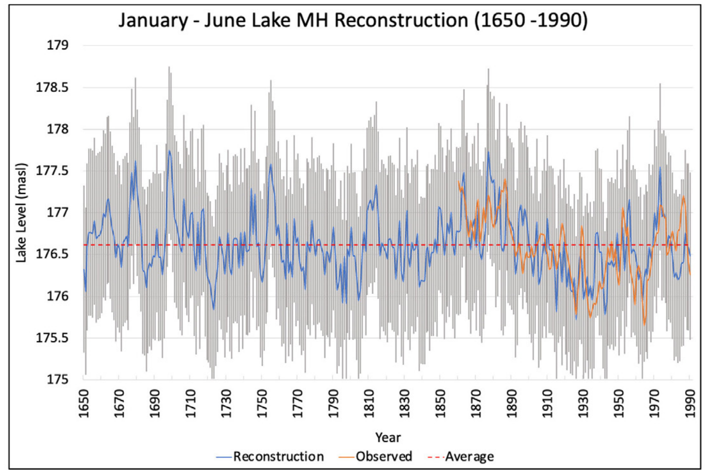

Figure 3. Reconstruction of January – June MH lake levels (1650 – 1990). Many of the early highs (1677, 1698, 1755, and 1810) are linked to volcanic eruptions and later highs and lows are linked to regional or global climate events. Blue line represents the reconstruction, orange line represents observed lake levels from 1860 to 1990, and gray bars represent the 95% confidence interval derived from the root squared mean error (RSME).

levels. Ten chronologies from Southeast Alaska were retained that were significantly correlated at the 0.01 confidence level for the full calibration period (Table 1). Each tree-ring series was also screened for time stability for the early (1866 – 1925) and late (1926–1990) calibration periods individually at the 0.01 level of significance.

RESULTS

The ten series used for full modeling in PCReg

Table 1. Correlation of S. Alaskan chronologies and lake levels (1860 – 1990).

SAMPLE	LAT.	LONG.	FIRST YEAR	LAST YEAR	SPECIES	CORREL.
COREYA	60.36	-145.40	1365	1992	TSME	r = 0.44
FULLTM	60.05	-150.01	1525	2004	TSME	r = 0.46
GNUNAT	61.05	-146.59	1410	2000	TSME	r = 0.29
MASSRK	60.38	-145.25	1508	1992	TSME	r = 0.52
MCGINN	58.26	-135.36	1380	1999	TSME	r = 0.51
RCKTOR	61.03	-147.06	1406	2002	TSME	r = 0.37
WITTIE	60.50	-148.35	1412	1991	TSME	r = 0.29
WOLVER	60.22	-148.54	1247	1991	TSME	r = 0.50
WRIGHT	58.45	-135.59	1552	2010	TSME	r = 0.52
YAKALS	59.33	-139.21	1576	1995	PCSI	r = 0.41

Notes: Southern Alaskan chronologies and their correlation with January – June MH lake levels (1860 – 1990). The ten ring-width chronologies used for modeling with first and last years are noted, along with latitudes and longitudes. TSME is Tsuga mertensiana (mountain hemlock) and PCSI is Picea sitchensis (Sitka spruce). R values are based on the correlation between January – June TRWs and MH lake levels from 1860 - 1990.

(Cook, E.R., 1990) were transformed into principal components, explaining 33.8% of the variance in January through June MH lake levels for the full calibration period. To assess the regression model, we calibrated two models using the first half of the lake level data (1860 – 1925) and the latter half of the data (1926 – 1990), explaining 33.3% and 27.6% of the variance, respectively (Table 2). After isolating the early and late periods of lake level data for modeling, we verified the model by calculating reduction of error (RE) and coefficient of error (CE) values. The positive RE values for both periods indicate that the model performs better than just using the mean of the calibration period as a predictor (Fritts et al., 1990). The CE value is slightly negative, indicating that the reconstruction does not outperform the mean of the verification period. However, positive RE and correlation values suggest the model retains predictive skill.

Table 2. Statistics for the Lake Michigan-Huron Reconstruction.

Calibration	Variance (%)	Reduction of Error (RE)	Coefficient of Efficiency (CE)
1860 - 1990	33.8		
1860 - 1925	33.3	0.343	-0.108
1926 – 1990	27.6	0.393	-0.216

Sign test (residual balance) results were favorable for the full reconstruction, with 68 positive residuals and 63 negative residuals, further verifying the model. The 131-year calibration period is also favorable for the model, as it captures most of the 20th century and nearly half of the 19th. The observed lake levels for January through June were compared with the reconstruction estimates and they exhibited a strong correlation (r = 0.58, N = 130 years).

DISCUSSION

Highs in the MH lake level reconstruction are attributed to volcanic eruptions and altered climate patterns (ENSO), whereas lows are linked to drought. Research in the GL has been done that correlates evaporation with ice cover (Van Cleave et al., 2014; Blanken et al., 2011), concluding that ice can act as a “lid” over lakes, keeping evaporation to a minimum. Due to the slow decay of volcanic aerosols and the reconstruction exhibiting high lake levels following eruptions, cooler temperatures from a lack of solar radiation likely increased ice cover and reduced evaporation on MH, contributing to higher lake levels in 1677, 1698, 1755, and 1810 following eruptions in 1673, the 1690s, 1755, and 1809 (Gao et al., 2008, D’Arrigo et al., 2013).

The reconstruction shows a peak in 1877 at 177.73 meters. From 1876 to 1878, the world experienced a series of droughts and consequent famine particularly in India, China, Egypt, Morocco, Ethiopia, Brazil, Colombia, and Venezuela (Singh et al., 2018). These extreme conditions correspond with the conditions produced by a very strong 2-year El Niño. Over the past 40 years with climate change, moisture contribution to the GL Region from the Mid-Pacific has increased significantly (Yang et al., 2023). During a typical El Niño (lasting 9-12 months; NOAA, 2016), the Pacific Jet Stream extends across the Southern US, bringing increased precipitation. During this very strong El Niño, it is possible that circulation patterns were altered and moisture from the Mid-Pacific was transported to the GL Region, leading to an increase in precipitation and MH lake levels from 1876 – 1878.

There is a low stand of MH lake levels from 1915 through 1963, likely due to temperature changes and dry conditions in the US. A series of droughts occurred in the 1930s through the 1950s due to changes in tropical Pacific SSTs, which affected global circulation, resulting in anomalies over North America (Seager et al., 2005). Also in the 1930s, the Great Plains experienced extreme drought eventually leading to the infamous Dust Bowl, which continued into the 1940s, providing further evidence of dry conditions in the US in the early 1900s (Seager et al., 2005). From about 1900 to 1950, there was a global temperature rise thought to be caused by an increase in greenhouse gases, a reduction in volcanic aerosols, or a small change in solar irradiance (Hegerl et al., 2018). This warming was caused by changes in SSTs, resulting in altered atmospheric patterns, like a decreased southerly inflow of moist air over the US (Hegerl et al., 2018). In 1973, the reconstruction shows another peak at 177.55 meters, attributed to above-normal precipitation in the GL Region from 1971 to 1974 because of wetter and cooler conditions in the GL basin (Stevens, 1973; Changnon, 1987).

CONCLUSIONS

The objective of this research was to build a well-verified reconstruction of historical MH lake levels. In summary, this study yields the following conclusions:

- Tree rings from Southeast Alaska capture climate variability relevant to MH levels.

- Calibration and verification statistics confirm a robust, well-verified 340-year reconstruction with a 131-year calibration period.

- Known climate conditions (volcanic eruptions, ENSO, drought, precipitation) compare well with the reconstruction model.

- Atmospheric climate patterns, volcanic forcing, and the PNA influence MH lake level fluctuations.

- Altered climate conditions influencing historical lake levels may help to inform lake level responses to climate change in the future.

- A strong ENSO event in 2026 may lead to increased lake levels in the coming years due to altered moisture patterns.

ACKNOWLEDGEMENTS

This material is based upon work supported by the Keck Geology Consortium and the National Science Foundation under Grant No. 2050697. I would like to thank Angoon's Alaskan Youth Stewards (AYS) for hosting our Keck research group, providing knowledge of the land, and accompanying us through many meaningful experiences on the island. I acknowledge that this research was conducted on the traditional lands of the Tlingit people and recognize and appreciate the deep connection of the Tlingit community to this land and its stewardship. I would also like to thank my student research partners for their collaboration and Dr. Wiles and Nick Wiesenberg for their continuous support on this project.

REFERENCES

Blanken, P. D., Spence, C., Hedstrom, N., & Lenters, J. D. (2011). Evaporation from Lake Superior: 1. Physical controls and processes. Journal of Great Lakes Research, 37(4), 707–716. https://doi.org/10.1016/j.jglr.2011.08.009

Brinkmann, W. A. R. (1992). Local tree-rings and teleconnections: Ways to improve the reconstruction of Lake Superior water supplies. Journal of Great Lakes Research, 18(3), 357–363. https://doi.org/10.1016/S0380-1330(92)71303-3

Changnon, S. (1987). Climate fluctuations and record-high levels of Lake Michigan. Bulletin of the American Meteorological Society. https://doi.org/10.1175/15200477(1987)068<1394:CFARHL>2.0.CO;2

Cook, E. R. (1985). A time series analysis approach to tree ring standardization (dendrochronology, forestry, dendroclimatology, autoregressive process) Retrieved from https://wooster.idm.oclc.org/login?url=https://www.proquest.com/dissertations-theses/time-series-analysis-approach-tree-ring/docview/303378100/se-2.

Dahlman, L. (2009). Climate variability: Pacific–North American pattern. NOAA. https://www.climate.gov/news-features/understanding-climate/climate-variability-pacific-north-american-pattern

D'Arrigo, R., Wilson, R., & Anchukaitis, K. J. (2013). Volcanic cooling signal in tree ring temperature records for the past millennium. Journal of Geophysical Research: Atmospheres, 118(16), 9000–9010. https://doi.org/10.1002/jgrd.50692

EPA. (2025). Great Lakes facts and figures. EPA. https://www.epa.gov/greatlakes/great-lakes-facts-and-figures

Fritts, H. C., Guiot, J., Gordon, G. A., & Schweingruber, F. (1990). Methods of calibration, verification, and reconstruction. In E. R. Cook & L. A. Kairiukstis (Eds.), Methods of dendrochronology (pp. 163–217). Springer Netherlands. https://doi.org/10.1007/978-94-015-7879-0_4

Gao, C., Robock, A., & Ammann, C. (2008). Volcanic forcing of climate over the past 1500 years: An improved ice core-based index for climate models. Journal of Geophysical Research: Atmospheres, 113(D23), 2008JD010239. https://doi.org/10.1029/2008JD010239

Ghanbari, R. N., & Bravo, H. R. (2008). Coherence between atmospheric teleconnections, Great Lakes water levels, and regional climate. Advances in Water Resources, 31(10), 1284–1298. https://doi.org/10.1016/j.advwatres.2008.05.002

Great Lakes Commission. (2026). About the lakes. Great Lakes Commission. https://www.glc.org/lakes/

Hegerl, G. C., Brönnimann, S., Schurer, A., & Cowan, T. (2018). The early 20th century warming: Anomalies, causes, and consequences. WIREs Climate Change, 9(4), e522. https://doi.org/10.1002/wcc.522

Meadows, G. A., Meadows, L. A., & Wood, W. L. (1997). The relationship between Great Lakes water levels, wave energies, and shoreline damages. Bulletin of the American Meteorological Society. https://doi.org/10.1175/1520-0477(1997)078<0675:TRBGLW>2.0.CO;2

Melvin, T. M., & Briffa, K. R. (2008). A “signal-free” approach to dendroclimatic standardisation. Dendrochronologia, 26(2), 71–86. https://doi.org/10.1016/j.dendro.2007.12.002

Melvin, T. M., & Briffa, K. R. (2014). CRUST: Software for the implementation of regional chronology standardisation: Part 1. Signal-free RCS. Dendrochronologia, 32(1), 7–20. https://doi.org/10.1016/j.dendro.2013.06.002

NOAA Physical Sciences Laboratory. (2012). 20CR Climate Indices: PNA. NOAA Physical Sciences Laboratory. https://psl.noaa.gov/data/20thC_Rean/timeseries/monthly/PNA/.

NOAA. (2026). Historic water levels—Station selection [Dataset]. https://tidesandcurrents.noaa.gov/stations.html?type=Historic+Water+Levels#Great%20Lakes%20-%20Lake%20Michigan

NOAA. (2026). Tides and currents [Dataset]. https://tidesandcurrents.noaa.gov/map/index.html?region=Lake%20Michigan

NOAA. (2026). Tree ring [Dataset]. https://www.ncei.noaa.gov/products/paleoclimatology/tree-ring

Popa, A., Popa, I., Roibu, C.-C., & Badea, O. N. (2022). Do different tree-ring proxies contain different temperature signals? A case study of Norway spruce (Picea abies (L.) Karst) in the Eastern Carpathians. Plants, 11(18), 2428. https://doi.org/10.3390/plants11182428

Quinn, F. H., & Sellinger, C. E. (2006). A reconstruction of Lake Michigan–Huron water levels derived from tree ring chronologies for the period 1600–1961. Journal of Great Lakes Research, 32(1), 29–39. https://doi.org/10.3394/0380-1330(2006)32[29:AROLMW]2.0.CO;2

Rodionov, S. (1994). Association between winter precipitation and water level fluctuations in the Great Lakes and atmospheric circulation patterns. Journal of Climate. https://doi.org/10.1175/1520-0442(1994)007<1693:ABWPAW>2.0.CO;2

Rogers, J. C., & Coleman, J. S. M. (2003). Interactions between the Atlantic Multidecadal Oscillation, El Niño/La Niña, and the PNA in winter Mississippi Valley stream flow. Geophysical Research Letters, 30(10), 2003GL017216. https://doi.org/10.1029/2003GL017216

Seager, R., Kushnir, Y., Herweijer, C., Naik, N., & Velez, J. (2005). Modeling of tropical forcing of persistent droughts and pluvials over Western North America: 1856–2000. Journal of Climate, 18(19), 4065–4088. https://doi.org/10.1175/JCLI3522.1

Singh, D., Seager, R., Cook, B. I., Cane, M., Ting, M., Cook, E., & Davis, M. (2018). Climate and the global famine of 1876–78. Journal of Climate, 31(23), 9445–9467. https://doi.org/10.1175/JCLI-D-18-0159.1

Stevens, W. (1973). Great lakes shore towns await ‘flood of the century.’ The New York Times. https://www.nytimes.com/1973/02/25/archives/great-lakes-shore-towns-await-flood-of-the-century-great-lakes.html

Van Cleave, K., Lenters, J. D., Wang, J., & Verhamme, E. M. (2014). A regime shift in Lake Superior ice cover, evaporation, and water temperature following the warm El Niño winter of 1997–1998. Limnology and Oceanography, 59(6), 1889–1898. https://doi.org/10.4319/lo.2014.59.6.1889

Wiles, G. C., Devereux, K., Gaglioti, B. V., & D’Arrigo, R. D. (2023). A 420-year perspective on winter Lake Erie levels. Geophysical Research

Letters, 50(1), e2022GL099911. https://doi.org/10.1029/2022GL099911

Yang, Z., Qian, Y., Xue, P., Wang, J., Chakraborty, T. C., Pringle, W. J., Li, J., & Chen, X. (2023). Moisture sources of precipitation in the Great Lakes region: Climatology and recent changes. Geophysical Research Letters, 50(5), e2022GL100682. https://doi.org/10.1029/2022GL100682

Learning Science Through Research
Published by the Keck Geology Consortium
Short Contributions
Keck Geology Consortium
Volume 38
May 2026
doi: 10.18277/AKRSG.2026.38.03

ANALYSIS OF MENDENHALL RIVER DISCHARGE AND A PRELIMINARY TREE-RING BASED RECONSTRUCTION

ISABEL HELD, Scripps College
Project Advisor: Robert Gaines

INTRODUCTION

Glaciated watersheds in Southeast Alaska are undergoing rapid change as rising temperatures deglaciate basins and alter the hydrology. The Mendenhall River, located near Juneau, Alaska, drains a basin that includes the Mendenhall Glacier. The Mendenhall Glacier has been retreating since the end of the Little Ice Age and in the last two decades has receded more than a kilometer and thinned up to 150 meters (Berthier, et al., 2018). The principal source of the river's discharge is glacial meltwater, making streamflow sensitive to summer temperature variability. As a result, summer discharge is linked to June through August temperatures and can be reconstructed using climate proxies such as temperature-sensitive tree rings.

In Southeast Alaska, tree-ring width chronologies are primarily sensitive to temperature changes and have been used to reconstruct temperature (Wiles et al., 2014), glacier mass balance (Malcomb and Wiles, 2013), and hydroclimate (Wiles et al., 2023). Higher summer temperatures drive glacial melt and tree growth, and thus tree growth can be used as a proxy for temperature change and glacier melt.

Glacial lake outburst floods (GLOFs) are common in this area, originating from an ice-dammed side basin of the glacier known as Suicide Basin (Fig. 1). GLOFs have occurred annually since 2011, producing record discharges and damaging homes and infrastructure in the Mendenhall Valley (NWS, 2025). The August 13, 2025 GLOF produced a record high flow, with the Mendenhall River cresting at 16.65 feet (NWS, 2025). Understanding the historical context of discharge variability is critical for anticipating future flood risk and informing adaptation. This study investigates the hydrologic and climatic dynamics of Mendenhall River and develops a preliminary tree-ring based streamflow reconstruction extending 200 years in the past.

STUDY AREA

The Mendenhall River originates from Mendenhall Lake at the terminus of the Mendenhall Glacier which lies approximately 19 kilometers North from downtown Juneau, Alaska (Fig. 1). The river flows through the Mendenhall Valley and empties into Fritz Cove. The basin receives inflow from tributaries such as Nugget Creek and Steep Creek, though glacial meltwater is the main source of the Mendenhall River's discharge. Juneau has a maritime climate with high annual precipitation, and the USGS has recorded continuous streamflow data at the Mendenhall River (15052500) gauging station in Auke Bay, Alaska

Figure 1. Map of the Mendenhall Valley with river, lake, and glacial features pictured (National Weather Service, 2018).

since 1966 (USGS, 1999). As part of the Keck-SEAK25 project's field season, the Mendenhall Trail tree-ring series originally sampled in 1999 was updated, expanding the chronologies' overlap with the discharge record.

METHODS

Annual discharge data was obtained from the USGS Auke Bay gauging station on the Mendenhall River from 1966 to 2024. Monthly minimum, maximum, and mean temperature records were obtained from the NOAA Global Historical Climatology Network (GHCN-Monthly) for the Juneau No. 2 station (NOAA NCEI, 2019). Correlations were calculated using KNMI Climate Explorer (Trouet & Van Oldenborgh, 2013). Pearson correlation coefficients were calculated between discharge and temperature across all calendar months.

A preliminary reconstruction of annual Mendenhall River discharge was developed using a principal component regression software called PCReg (Cook, 1985). Using PCReg, a combination of twelve Alaskan tree ring width series was compared to the annual discharge of the Mendenhall River. The twelve Alaskan tree-ring were significantly correlated (Fig. 2; $p < 0.05$), serving as predictors of annual discharge. The first two principal components of the tree ring chronologies were used as predictors and the discharge (the predictand) was then used to calibrate a model to reconstruct past average yearly discharge (Fig. 3).

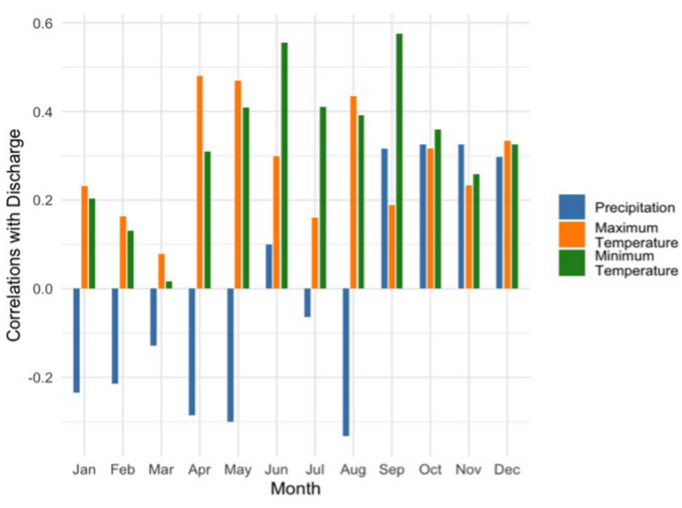

Figure 2. Correlation coefficients between monthly climate variables (minimum temperature, maximum temperature and precipitation) and monthly Mendenhall River discharge.

The calibration period spanned 1966–2000 (n = 35 years). The model was evaluated using the Pearson correlation between reconstructed and observed discharge values. The regression model was then applied to the full length of the chronologies to create a 200 year annual reconstruction. Spatial correlations between reconstructed and observed discharge against gridded minimum temperature fields were compared to assess the geographic coherence of the reconstruction signal (Fig. 4).

RESULTS

Discharge Trends and Climate Correlations

The discharge of the Mendenhall River has been increasing since the mid-1970's (Fig. 3), with higher summer discharges due to increases in Mendenhall Glacier melting during June, July, and August. Annual discharge of the Mendenhall River has increased by approximately 430 cfs between 1966 and 2024, with the most pronounced increases occurring in summer months (June-August), consistent with accelerated glacial melt (Fig. 3). Discharge displays strong positive correlations with monthly minimum, maximum, and mean temperatures in Juneau throughout the summer melt season. Precipitation is a less consistent predictor of discharge with fluctuating positive and negative correlations throughout the year (Fig. 2).

Preliminary Reconstruction

The twelve Alaskan tree-ring chronologies collectively explain over 40% of the variance in annual Mendenhall River discharge over the calibration period. Reconstructed and observed discharge values are significantly correlated ($r = 0.70$, $n = 35$, 95% CI = +/- 0.14), supporting the use of tree rings for a preliminary reconstruction (Fig. 3). The extended reconstruction suggests that several 21st-century discharges - particularly those associated with GLOF events - are exceptional in the context of the past 200 years.

DISCUSSION

The strong temperature-discharge relationship at the Mendenhall River is consistent with the glacier-

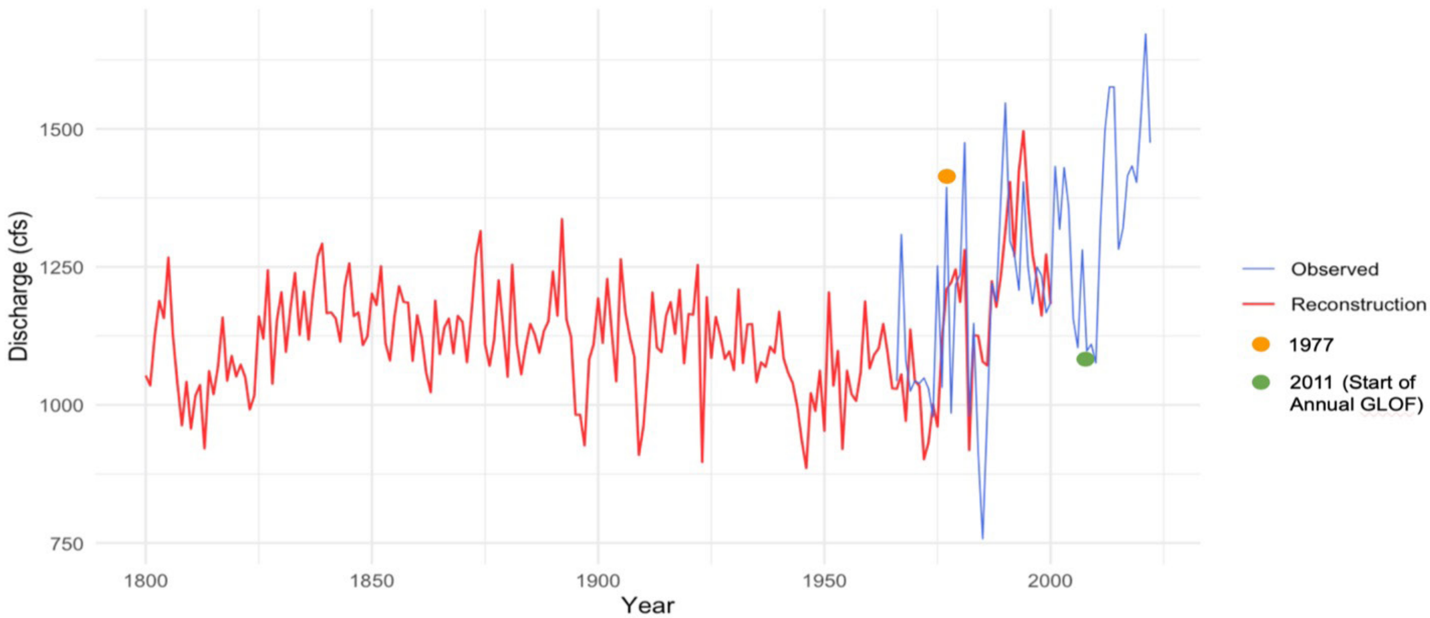

Figure 3. Preliminary reconstruction of annual Mendenhall River discharge in red (ca. 1800-2000). Observed discharge in cfs (1966-2000) shown for comparison in blue.

dominated hydrology of the basin. As summer temperatures rise, accelerated melt of the Mendenhall Glacier directly increases river discharge. This same temperature signal is found in tree-ring width chronologies across Alaska, where ring growth is primarily temperature-limited (Wiles et al., 2014). Therefore, the correlation between ring widths and discharge reflects a shared climate driver - summer temperature.

A major climatic regime shift in 1976-77, associated with a phase transition of the Pacific Decadal Oscillation (PDO) from cool to warm, corresponds with a step increase in Juneau temperatures, precipitation, and Mendenhall River discharge. This shift is evident in both the observational record and in the reconstructed discharge series, lending additional confidence to the reconstruction's ability to capture hydroclimatic variability.

The extended reconstruction places recent high-discharge years in a 200-year context. The finding that multiple 21st-century discharges appear unmatched in the reconstructed record suggests that current discharge levels reflect both climate variability and a sustained shift towards higher baseline discharge driven by accelerating glacial melt. This trend is projected to continue under future warming. Spatial correlations between reconstructed and observed discharge against minimum temperature fields display

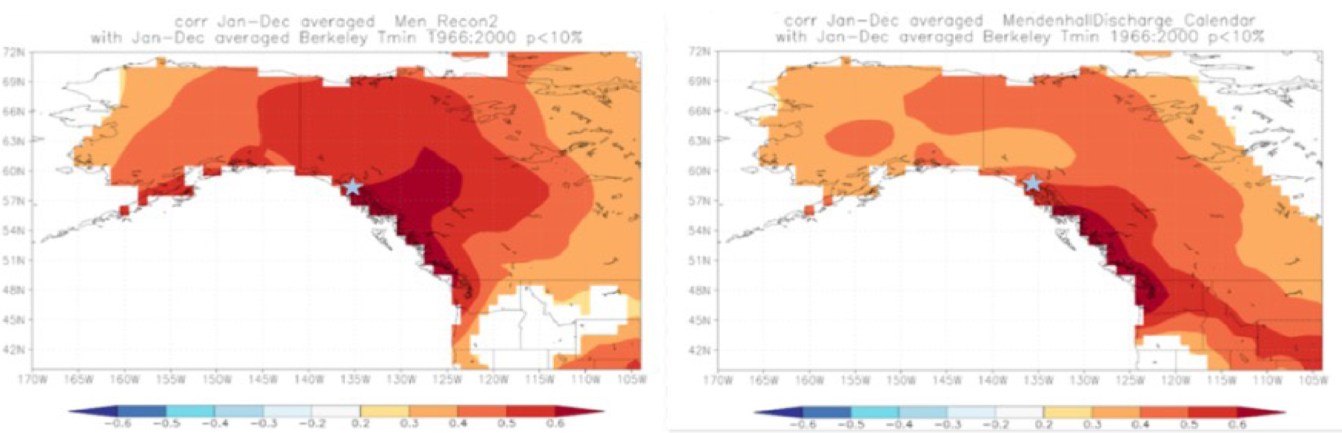

Figure 4. Left) Heatmap of correlations between reconstructed discharge and Tmin. Right) Heatmap of correlations between observed discharge and Tmin. Blue star overlies Juneau, AK.

similar geographic patterns, providing additional validation of the reconstruction (Fig. 4).

CONCLUSIONS

This study demonstrates that Mendenhall River discharge is strongly controlled by summer temperatures, consistent with the glacier-dominated hydrology of the basin. Tree-ring chronologies from Alaska capture this temperature signal and serve as proxies for annual streamflow. A preliminary reconstruction based on twelve Alaskan tree ring width chronologies explains over 40% of discharge variance and correlates strongly with observed values ($r = 0.70$, $n = 35$). The extended record suggests that recent high-discharge years are exceptional in a 200-year context, likely reflecting the combined influence of a 1977 PDO regime shift and glacial retreat. Future work should update the Alaskan tree-ring chronologies to extend the calibration period, and apply formal verification statistics to improve the accuracy of future reconstructions. These findings underscore the importance of long-term hydroclimatic context for anticipating flood risk in the Mendenhall Valley.

ACKNOWLEDGEMENTS

This material is based upon work supported by the Keck Geology Consortium and the National Science Foundation under Grant No. 2050697. Thank you to Dr. Greg Wiles for the thoughtful edits and dendrochronology expertise throughout this process. Thank you Nick Wiesenberg for the hospitality in Wooster and always lending a helping hand. Thank you Lynnsey, Dexter, Lev and Landon - I feel really lucky to have had such an upbeat and smart cohort to collaborate with. Thank you Bob Gaines for the great advice and edits back at Pomona College. Thank you S'eiltin Jamiann Hasselquist for the guidance on Tlingit-Haida history. Thank you to the Angoon community as a whole for their generosity and hospitality.

REFERENCES

Berthier, E., Larsen, C., Durkin, W.J., Willis, M.J., and Pritchard, M.E., 2018, Brief communication: Unabated wastage of the Juneau and Stikine icefields (southeast Alaska) in the early 21st century: The Cryosphere, v. 12, p. 1523–1530, doi:10.5194/tc-12-1523-2018.

Cook, E. R. (1985). A Time Series Analysis Approach to Tree Ring Standardization. PhD thesis, The University of Arizona.

Kienholz, C., Amundson, J.M., Motyka, R.J., Jackson, R.H., Truffer, M., Stuefer, S.L., Nash, J.D., Kress, A., Campbell, C., and Larsen, C.F., 2020, Deglacierization of a Marginal Basin and Implications for Outburst Floods, Mendenhall Glacier, Alaska: Frontiers in Earth Science, v. 8, doi:10.3389/feart.2020.00137.

Malcomb, N.L., and Wiles, G.C., 2013, Tree-ring-based reconstructions of North American glacier mass balance through the Little Ice Age - Contemporary warming transition: Quaternary Research, v. 79, p. 123–137, doi:10.1016/j.yqres.2012.11.005.

Motyka, R.J., O'Neel, S., Connor, C.L., and Echelmeyer, K.A., 2003, Twentieth century thinning of Mendenhall Glacier, Alaska, and its relationship to climate, lake calving, and glacier run-off: Global and Planetary Change, v. 35, p. 93–112, doi:10.1016/S0921-8181(02)00138-8

National Weather Service, 2018, Map of Suicide Basin: National Weather Service, https://www.weather.gov/ajk/suicidebasin (accessed April 2026).

National Weather Service (NWS), 2025, Suicide Basin Monitoring and Current Conditions: National Oceanic and Atmospheric Administration, Juneau, AK, https://www.weather.gov/ajk/suicidebasin (accessed April 2026).

NOAA National Centers for Environmental Information, 2019, GHCN-Monthly temperature data for JUNEAU NO 2 (Station ID: 70381): U.S. National Oceanic and Atmospheric Administration, https://www.ncei.noaa.gov/products/land-based-station/global-historical-climatology-network-monthly (accessed October 2025).

Trouet, V., and Van Oldenborgh, G.J., 2013, KNMI Climate Explorer: a web-based research tool for high-resolution paleoclimatology: Tree-Ring Research, v. 69, no. 1, p. 3–13, doi:10.3959/1536-1098-69.1.3.

U.S. Geological Survey (USGS), 1999, Hydrology, geomorphology, and flood profiles of the Mendenhall River, Juneau, Alaska: U.S. Geological Survey Water-Resources Investigations Report 99-4150, 1 sheet, doi:10.3133/wri994150.

Wiles, G.C., Devereux, K., Gaglioti, B.V., and D'Arrigo, R.D., 2023, A 420-Year Perspective on Winter Lake Erie Levels: Geophysical Research Letters, v. 50, no. 1, doi:10.1029/2022GL099911.

Wiles, G.C., Solomina, O., D'Arrigo, R.D., Anchukaitis, K., Gensiarovsky, Y., and Wiesenberg, N., 2014, Reconstructed Summer Temperatures over the Last 400 Years Based on Larch Ring Widths: Sakhalin Island, Russian Far East: Climate Dynamics, v. 43, p. 111–125, doi:10.1007/s00382-014-2209-2.

KECK Geology Consortium
Learning Science Through Research
Published by the Keck Geology Consortium
Short Contributions
Keck Geology Consortium
Volume 38
May 2026
doi: 10.18277/AKRSG.2026.38.04

INVESTIGATING THE INDIAN OCEAN DIPOLE–NORTHEAST PACIFIC TELECONNECTION WITH TREE-RING CHRONOLOGIES FROM ALASKA

DEXTER C. PAKULA, Carleton College
Project Advisor: Cameron Davidson

INTRODUCTION

The skill of seasonal climatic prediction in the United States is relatively low because predictable signals are weak relative to internally generated midlatitude atmospheric variability (O'Lenic et al., 2008; Peng et al., 2012, 2013). Dominant climate modes such as the El Niño Southern Oscillation (ENSO), the Pacific Decadal Oscillation (PDO), and the Atlantic Multidecadal Variability (AMV) offer sources of predictable variability but exhibit temporal nonstationary and varying regional effects (Fernández-Castillo et al., 2025; Rohli et al., 2022). Recent studies have investigated additional climate modes and teleconnections from the tropics, such as the Indian Ocean Dipole (IOD), for sources of further predictable variability (Molteni and Brookshaw, 2024).

IOD teleconnections with the extratropics are driven by large-scale sea-surface temperature (SST) anomalies associated with an IOD event, which induce diabatic heating and excite Rossby wave trains propagating over the North Pacific (Hoskins and Karoly, 1981; McIntosh and Hendon, 2018). This influences semi-permanent pressure systems and mid-tropospheric circulation across North America and the North Atlantic (Bader and Latif, 2005; Branstator, 2002; Hu et al., 2023; Min et al., 2008). IOD teleconnections have been studied for impacts on the North Atlantic Oscillation (NAO) in early winter and climatic predictive value in Europe (Abid et al., 2023; Fereday et al., 2025; Hardi man et al., 2020; Raganato et al., 2025). Despite this attention, few studies have investigated the linkage between the IOD and North American climate (Min et al., 2008; Saji and Yamagata, 2003). One approach is to examine the climate-sensitive Northeast Pacific coastal and near-coastal tree-ring record to explore teleconnection signals from the Indian Ocean (D'Arrigo et al., 2005).

The goal of this study is to improve the understanding of the IOD–North America teleconnection using tree-ring width records from the Northeast Pacific and by utilizing the Dipole Mode Index (DMI), which characterizes the IOD. The central aims are to determine if the teleconnection signal is present in the tree-ring record from Alaska, independent of ENSO, and temporally stationary over the past few centuries. I present extended and optimized chronology network reconstructions of the DMI and the DMI with ENSO influence removed (rDMI), allowing for analysis of the teleconnection structure and the reconstruction predictive skill.

METHODS

Tree-ring Data

I utilized a dataset of 182 tree-ring width chronologies from Alaska, assembled by The College of Wooster Tree Ring Lab (WTRL). Chronologies were detrended with the signal-free approach using RCSig (Cook et al., 2017), which estimates growth-related trends while accounting for shared signals among chronologies, reducing detrending biases (Melvin and Briffa, 2008, 2014).

Chronologies were correlated with the DMI and rDMI, and those exhibiting statistically significant correlations ($p < 0.05$) for the common interval (1870-1980 CE) were retained for modeling (Fig. 1). Eighty-three chronologies were retained (Fig. 1), all of which span1835–1980 CE and are most strongly correlated

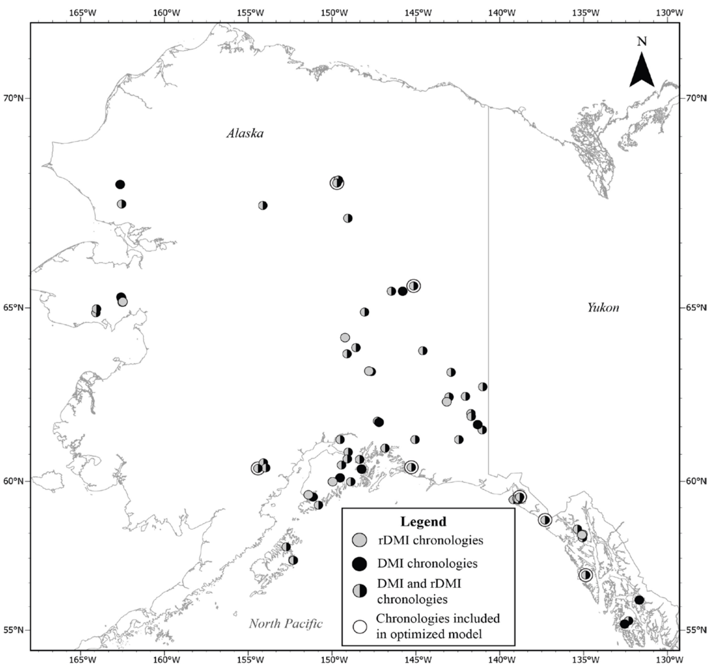

Figure 1. Locations of the tree-ring chronologies included in this study. Of the 83 total chronologies, 13 passed only the DMI screening, eight passed only the rDMI screening, and 62 passed both screenings. The chronologies marked with white circles were retained for the optimized-chronology models.

with average January–March indices (JFM; Fig. 2).

Climate Data

The SST climate data is derived from HadiSST1, which spans 1870-2025 (Rayner et al., 2003). The DMI is the SST anomaly difference between the Western Tropical Indian Ocean (WTIO; 50° E–70° E, 10° S–10° N) and the Southeastern Tropical Indian Ocean (SETIO; 90° E–110° E, 10° S–Equator; Saji et al., 1999). The Niño3.4 index represents ENSO with the average SST anomalies in the region (170° W–120° W, 5° S–5° N; Rayner et al., 2003). The rDMI was calculated by linearly regressing Niño3.4 on the DMI and retaining the residuals as a new dataset. This removes the linear portion of the influence of ENSO from the DMI.

Gridded climate datasets were used for field correlations with the principal components (PCs) derived from the chronologies that passed screening for both models. The gridded data include the HadCRUT 5.0 land and sea temperatures (Morice et al., 2021) and 500 hPa meridional wind variability and geopotential height from the NOAA 20th Century Reanalysis Version 3 monthly 2° × 2° fields (1851–2014; NOAA Physical Sciences Laboratory, 2024). These were used to explore linkages by revealing the Rossby wave structure via surface and atmospheric expressions. All climate data were acquired through the Koninklijk Nederlands Meteorologisch Instituut (2022; Trouet and Van Oldenborgh, 2013).

STATISTICAL MODELS

PC-based reconstructions were generated from the network of 83 chronologies using the principal component regression software PCreg (Cook and Krusic, n.d.). Reconstructions were calibrated over the common period between the SST data and the tree-ring data (1870–1980), modeling index values averaged over an optimal monthly interval determined from regression trials across the dendroclimatic year. Parallel reconstructions of the DMI and rDMI under the same model parameters were built to allow for isolation of the influence of ENSO on the teleconnection.

DMI Model

The DMI reconstruction was built to assess the linkage of Alaskan tree growth and Indian Ocean SST variability under the influence of ENSO. This reconstruction used 75 of the 83 chronologies and is referred to as “extended” because chronologies were included regardless of temporal stationarity (Fig. 1).

A secondary reconstruction of the DMI was built using principal component regression of a temporally stationary subset of the 75 chronologies (Fig. 1). These were identified using split-period calibration trials (1870–1925 and 1926–1980); chronologies that exhibited statistically significant correlations ($p < 0.05$) with the target index in both intervals were retained as a new dataset, and PCs were recomputed. While the extended chronology reconstruction is useful for assessing the structure of the teleconnection, the optimized one is useful for quantifying predictive skill, because it is restricted to chronologies that are consistently tuned to climate signals from the Indian Ocean throughout the modeled interval.

rDMI Model

The rDMI was reconstructed to isolate the component of the teleconnection independent of ENSO. The same processes were applied to the rDMI as were to the DMI for both extended and optimized reconstructions, though the extended reconstruction used 70 of the 83 chronologies (Fig. 1).

Model Assessment

Model assessment was conducted separately for the extended and optimized reconstructions to evaluate temporal stationarity and predictive skill, respectively. Running correlations between the reconstructions and the target index over a 30-year centered window were used to investigate the temporal stationarity of the extended models. Correlation coefficients were considered statistically significant if they exceeded a $p < 0.05$ threshold based on the two-sided Student's t-test. Predictive value of the optimized reconstructions was computed using split-period verification statistics, including the Pearson r, p-value, reduction of error (RE), and coefficient of efficiency (CE).

RESULTS

Teleconnection Signal

Principal component regression of the 182-chronology tree-ring series on the monthly DMI and rDMI over the calibration period (1870-1980) showed the strongest relationship ($R^2 > 0.28$) in January-March (JFM; Fig. 2), which restricted the final regression models to JFM (Fig. 3). A similar interval (December-May) was used for regression in D'Arrigo et al. (2005).

DMI Model

The extended JFM DMI reconstruction is shown in the upper panel of Figure 3a. The model uses 75 chronologies and five PCs to explain 39.5% of the variance in the index. The lower panel of Figure 3a is a running correlation plot, showing the 30-year averaged moving correlations throughout the modeled interval. The correlations drop below the 95% confidence interval from around 1891–1900, 1927–1932, and 1947–1952.

Five chronologies passed the criteria for the optimized

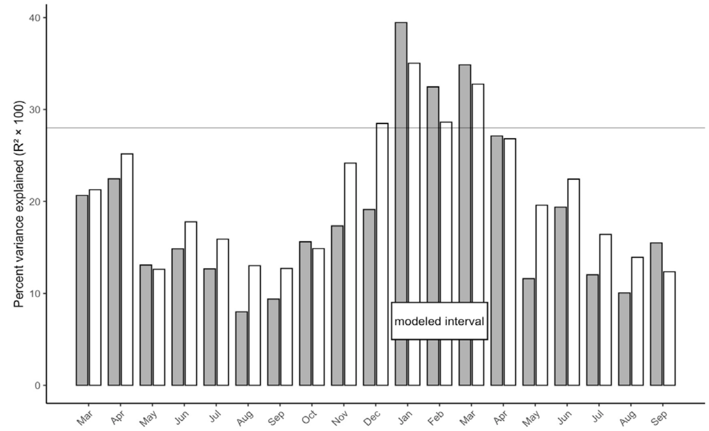

Figure 2. Monthly correlations of the model values with the corresponding index values from the DMI and rDMI between 1870 and 1980. The grey bars represent the correlations of the DMI model with the DMI, and the white bars represent the correlations of the rDMI model with the rDMI.

DMI model (Table 1), and the reconstruction used one PC to explain 40.6% of the variance in the index. Half-calibration window regression trials revealed the optimized DMI model explains 34.3% of the variance in the first period, and 24.8% in the second. The RE and CE statistics indicate robust predictive value (RE and CE > 0) across both intervals (Table 1).

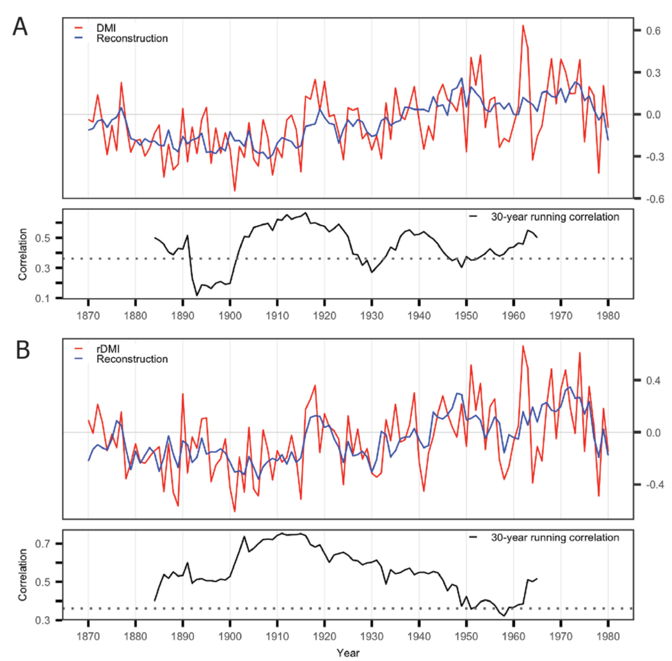

Figure 3. (A) The 75 chronology reconstruction (blue) of the JFM DMI, plotted against the index values (red). (B) The 70 chronology reconstruction (blue) of the JFM rDMI, plotted against the index values (red). Both plots include a 30-year running correlation between the model values and the index values (black). Values above the dotted line are statistically significant ($p < 0.05$).

Table 1. Verification statistics for optimized DMI and rDMI models

Model	Verification period	Pearson *r*	*p*	RE	CE	Durbin-Watson
DMI	1926–1980	0.510	<0.001	0.55	0.24	2.00
DMI	1870–1925	0.560	<0.001	0.66	0.29	1.90
rDMI	1926–1980	0.468	<0.001	0.41	0.19	2.07
rDMI	1870–1925	0.527	<0.001	0.50	0.23	2.03

*Verification statistics calculated using split-period calibration/verification. RE = reduction of error; CE = coefficient of efficiency.

rDMI model

The extended JFM rDMI model (Fig. 3b) uses 70 chronologies and six PCs to explain 39.7% of the variance in the index. The running correlation dips below the 95% confidence interval in the late 1950s.

Four chronologies were retained for the optimized rDMI model (Table 1). The reconstruction used one PC to explain 29.9% of the variance in the index for the whole calibration period, 32.8% in the first half, and 27.1% in the second half. The verification statistics indicate robust predictive skill (RE and CE > 0) in both intervals (Table 1).

The DMI and rDMI extended chronology reconstructions support a statistically significant linkage between tree growth in Alaska and the JFM DMI. While the extended DMI and rDMI models explain similar percentages of the variance in their target indices, the optimized models and verification statistics reveal that the DMI model possesses stronger predictive skill.

Principal Components

I computed field correlations between PC1 and PC2 (Fig. 4) of the extended DMI model and gridded climate datasets. Figure 4 is restricted to the DMI, though for both PCs, the DMI and rDMI extended models show roughly inverse patterns. PC1 shows strong negative correlations with land/SSTs in the WTIO, eastern Asia, the North Pacific, and the Atlantic tropics and extratropics. PC1's correlations with the 500 hPa meridional winds manifest as latitudinally and longitudinally alternating positive and negative fields concentrated in the Pacific. The 500 hPa geopotential height field shows a strong correlation on the coast of East Asia, and a weaker correlation to the east on the same latitude (around 30°–50°N), as well as a negative correlation field in the South Pacific.

Across all variables, the field correlations with PC1 are stronger and more widespread than with PC2. PC2's surface temperature correlation plot shows a positive field extending eastward from Japan. The 500 hPa meridional winds and geopotential height show weaker correlations, though similar patterns to PC1.

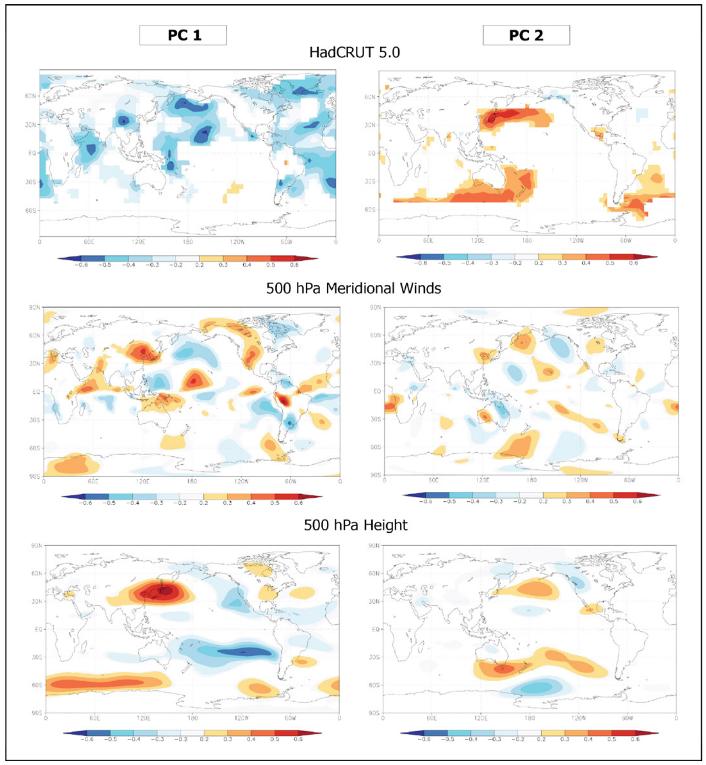

Figure 4. Extended DMI model PC1 (left) and PC2 (right) field correlations. Red indicates positive correlations, blue indicates negative correlations. The top row is correlated against land surface temperature and SST data, the middle row against 500 hPa meridional winds, and the bottom row against 500 hPa height.

DISCUSSION

The reconstructions indicate a statistically significant and moderately strong teleconnection between Alaskan tree growth and the January–March (JFM) Dipole Mode Index (DMI), with the optimized models demonstrating robust predictive skill. However, the strength of the relationship may vary through time. Here, I discuss the teleconnection strength, the role of ENSO, temporal stationarity, and principal component results.

Teleconnection Strength

The extended reconstructions (Fig. 3) explain approximately 40% of the variance in the DMI and rDMI, indicating a moderate, robust relationship between Alaskan tree growth and Indian Ocean SST variability. This level of explained variance is comparable to values often obtained in dendroclimatic reconstructions of large-scale climate mode indices. Despite substantial internal variability in the midlatitude climate system, the teleconnection signal is sufficiently strong to be expressed in the tree-ring width record.

The Role of ENSO

One of the central goals of this study was to determine if a unique teleconnection exists in the absence of ENSO. Comparing the percentages of variance explained by the extended models suggests the teleconnection is not driven by ENSO; the full rDMI model explains a marginally higher percentage of the variance than the full DMI model. However, the optimized DMI model explains the highest percent variance of all models, whereas the optimized rDMI model explains the lowest percent variance; once reduced to the temporally stationary chronologies, the DMI model is strengthened, and the rDMI model is weakened. Additionally, the verification statistics reveal that the optimized DMI model is more robust than the optimized rDMI model (Table 1). ENSO likely plays a role in the teleconnection, though it is unlikely that it drives the observed linkages.

Temporal Stationarity

The sample size for the optimized models is greatly reduced from the full models (Fig. 1), indicating non-stationary tree-growth patterns with respect to the Indian Ocean Dipole (IOD). The robust RE and CE statistics partially reconcile this, though the values are lower in the latter verification interval for both models (Table 1). The running correlation plots (Fig. 3) show similar patterns–the correlations peak in the early 1900s. The DMI correlation plot shows cyclic phases of high correlations and low correlations after the early 1900s on a decadal timescale (Fig. 3a), aligning well with PDO phase changes (Mantua and Hare, 2002). The full rDMI plot shows a steady decrease without cyclicity from around 1925–1960 (Fig. 3b), aligning well with Atlantic Multidecadal Variability (AMV) phase changes (Enfield et al., 2001). Overall, the models are reasonably stationary–the teleconnection signal is rarely absent, though most of the included chronologies fail to consistently display the signal between 1870 and 1980, and large-scale climate phase changes may impact the strength of the signal.

Principal Components

The field correlations for PC1 of the DMI model show coherent, evenly spaced correlation zones (Fig. 4). The land/SST correlation plot shows two distinct negative correlation field arcs and may be the surface expression of planetary waves. In the propagation phase, Rossby waves often exhibit an arc shape prior to being guided by the jet stream and constrained to the extratropics (Branstator, 2002). The 500 hPa meridional winds show alternating zones of northerly and southerly 500 hPa winds, which is evidence of wave nodes. The 500 hPa geopotential height field plot indicates longitudinal ridge and trough topography, which is characteristic of Rossby waves, particularly in conjunction with the meridional winds pattern (Wallace and Gutzler, 1981).

The field correlations for PC2 are weaker and less widespread than those for PC1. The PC2 500 hPa meridional winds and height show a similar structure to the PC1 correlations. The PC2 land/SST field correlation exhibits a PDO-type structure, with no evidence for planetary waves. Overall, the field correlations reveal Rossby wave structure, providing additional evidence for the presence of a teleconnection linking the Indian Ocean to the Gulf of Alaska.

CONCLUSIONS

Overall, the models explain a convincing portion of the variance in the climate indices, suggesting the presence of a teleconnection linking the climate in the Northeast Pacific to the January-March (JFM) Indian Ocean Dipole (IOD). The verification statistics for the optimized models indicate that select Alaskan trees have robust predictive skill of the JFM Dipole Mode Index (DMI). The presence of a teleconnection linking the JFM DMI to the climate in the Northeast Pacific may be a valuable insight for seasonal climate prediction in North America, if the precise climatic effects can be constrained and differentiated from other Indian Ocean teleconnection signals.

ACKNOWLEDGMENTS

This material is based upon work supported by the Keck Geology Consortium and the National Science Foundation under Grant No. 2050697. I would like to thank my fellow Keck Geology Consortium researchers for many thoughtful discussions and for the time we spent together in the field, all of which helped shape this work. The ongoing support throughout the research and writing process from Greg Wiles, Cam Davidson, and Dan Maxbauer was critical for producing and refining the presented results. I am grateful for the dedication of Greg Wiles and Nick Wiesenberg to sharing the art and science of dendrochronology, and the countless lessons I learned from them both in the lab and in the field.

REFERENCES

Abid, M. A., F. Kucharski, F. Molteni, and M. Almazroui (2023), Predictability of Indian Ocean precipitation and its North Atlantic teleconnections during early winter, npj Climate and Atmo spheric Science, 6 (1), 17, doi:10.1038/s41612-023-00328-z.

Bader, J., and M. Latif (2005), North Atlantic Oscillation response to anomalous Indian Ocean SST in a coupled GCM, Journal of Climate, 18 (24), 5382–5389, doi:10.1175/JCLI3577.1.

Branstator, G. (2002), Circumglobal teleconnections, the jet stream waveguide, and the North At lantic Oscillation, Journal of Climate, 15 (14), 1893–1910, doi:10.1175/1520-0442(2002)015<1893:CTTJSW>2.0.CO;2.

Cook, E. R., and P. J. Krusic (n.d.), PcReg, Computer program, Lamont-Doherty Earth Observatory and University of Cambridge dendrochronology software archive.

Cook, E. R., P. J. Krusic, K. Peters, and T. M. Melvin (2017), Program SignalFree: RCS signal-free tree-ring standardization program.

D'Arrigo, R., R. Wilson, C. Deser, G. Wiles, E. R. Cook, R. Villalba, A. Tudhope, J. Cole, and B. Linsley (2005), Tropical–North Pacific climate linkages over the past four centuries, Journal of Climate, 18 (24), 5253–5265, doi:10.1175/JCLI3602.1.

Enfield, D. B., A. M. Mestas-Nuñez, and P. J. Trimble (2001), The atlantic multidecadal oscillation and its relation to rainfall and river flows in the continental u.s., Geophysical Research Letters, 28 (10), 2077–2080, doi:10.1029/2000GL012745.

Fereday, D. R., J. R. Knight, and A. A. Scaife (2025), Climate change alters the Indian Ocean Dipole and weakens its North Atlantic teleconnection, Communications Earth & Environment, 6 (1), 152, doi:10.1038/s43247-025-02131-5.

Fernández-Castillo, P., T. Losada, B. Rodríguez-Fonseca, D. García-Maroto, E. Mohino, and L. Durán (2025), Multidecadal variability of the ENSO early-winter teleconnection to Europe and implications for seasonal forecasting, npj Climate and Atmospheric Science, 8 (1), 272, doi: 10.1038/s41612-025-01160-3.

Hardiman, S. C., N. J. Dunstone, A. A. Scaife, D. M. Smith, J. R. Knight, P. Davies, M. Claus, and R. J. Greatbatch (2020), Predictability of European winter 2019/20: Indian Ocean Dipole impacts on the NAO, Atmospheric Science Letters, 21 (12), e1005, doi:10.1002/asl.1005.

Hoskins, B. J., and D. J. Karoly (1981), The steady linear response of a spherical atmosphere to thermal and orographic forcing, Journal of the Atmospheric Sciences, 38 (6), 1179–1196, doi: 10.1175/1520-0469(1981)038<1179:TSLROA>2.0.CO;2.

Hu, Z.-Z., A. Kumar, B. Jha, M. Chen, and W. Wang (2023), The tropical Indian Ocean matters for U.S. winter precipitation variability and predictability, Environmental Research Letters, 18 (7), doi:10.1088/1748-9326/ace06e.

Koninklijk Nederlands Meteorologisch Instituut (KNMI) (2022), KNMI Climate Explorer, Available at https://climexp.knmi.nl/start.cgi, accessed 17 November 2025.

Mantua, N. J., and S. R. Hare (2002), The pacific decadal oscillation, Journal of Oceanography, 58 (1), 35–44, doi:10.1023/A:1015820616384.

McIntosh, P. C., and H. H. Hendon (2018), Understanding Rossby wave trains forced by the Indian Ocean Dipole, Climate Dynamics, 50 (7-8), 2783–2798, doi:10.1007/s00382-017-3771-1.

Melvin, T. M., and K. R. Briffa (2008), A "signal-free" approach to dendroclimatic standardisation, Dendrochronologia, 26 (2), 71–86, doi:10.1016/j.dendro.2007.12.001.

Melvin, T. M., and K. R. Briffa (2014), CRUST: Software for the implementation of regional chronol ogy standardisation: Part 2. Further RCS options and recommendations, Dendrochronologia, 32 (4), 343–356, doi:10.1016/j.dendro.2014.07.008.

Min, J., Q. Zhou, N. Liu, Q. Gao, and Z. Guan (2008), Teleconnection mode between IOD and northern hemisphere tropospheric circulation and its mechanism, Meteorology and Atmospheric Physics, 100 (1), 207–215, doi:10.1007/s00703-008-0304-9.

Molteni, F., and A. Brookshaw (2024), Indian Ocean teleconnections to the northern extra-tropics, ECMWF Technical Memorandum 923, European Centre for Medium-Range Weather Forecasts, Reading, UK.

Morice, C. P., J. J. Kennedy, N. A. Rayner, J. P. Winn, E. Hogan, R. E. Killick, R. J. H. Dunn, T. J. Osborn, P. D. Jones, and I. R. Simpson (2021), An updated assessment of near-surface temperature change from 1850: The HadCRUT5 data set, Journal of Geophysical Research: Atmospheres, 126, e2019JD032,361, doi:10.1029/2019JD032361.

NOAA Physical Sciences Laboratory (2024), NOAA 20th century reanalysis version 3 (2° × 2°, 1851–2014), accessed 15 February 2026.

O'Lenic, E. A., D. A. Unger, M. S. Halpert, and K. S. Pelman (2008), Developments in operational long-range climate prediction at CPC, Weather and Forecasting, 23 (3), 496–515.

Peng, P., A. Kumar, M. S. Halpert, and A. G. Barnston (2012), An analysis of CPC's operational 0.5-month lead seasonal outlooks, Weather and Forecasting, 27 (4), 898–917.

Peng, P., A. G. Barnston, and A. Kumar (2013), A comparison of skill between two versions of the NCEP Climate Forecast System (CFS) and CPC's operational short-lead seasonal outlooks, Weather and Forecasting, 28 (2), 445–462.

Raganato, A., M. A. Abid, and F. Kucharski (2025), The combined link of the Indian Ocean Dipole and ENSO with the North Atlantic–European circulation during early boreal winter in reanalysis and the ECMWF SEAS5 Hindcast, Journal of Climate, 38 (2), 445–460, doi: 10.1175/JCLI-D-23-0703.1.

Rayner, N. A., D. E. Parker, E. B. Horton, C. K. Folland, L. V. Alexander, D. P. Rowell, E. C. Kent, and A. Kaplan (2003), Global analyses of sea surface temperature, sea ice, and night marine air temperature since the late nineteenth century, Journal of Geophysical Research: Atmospheres, 108 (D14), doi:10.1029/2002JD002670.

Rohli, R. V., G. A. Snedden, E. R. Martin, and K. L. DeLong (2022), Impacts of ocean-atmosphere teleconnection patterns on the south-central United States, Frontiers in Earth Science, Volume 10 - 2022, doi:10.3389/feart.2022.934654.

Saji, N. H., and T. Yamagata (2003), Possible impacts of the Indian Ocean dipole mode events on global climate, Climate Research, 25 (2), 151–169.

Trouet, V., and G. J. Van Oldenborgh (2013), KNMI Climate Explorer: A web-based research tool for high-resolution paleoclimatology, Tree-Ring Research, 69 (1), 3–13, doi:10.3959/1536-1098-69.1.3.

Wallace, J. M., and D. S. Gutzler (1981), Teleconnections in the geopotential height field dur ing the northern hemisphere winter, Monthly Weather Review, 109 (4), 784–812, doi:10.1175/1520-0493(1981)109<0784:TITGHF>2.0.CO;2.

KECK Geology Consortium
Learning Science Through Research
Published by the Keck Geology Consortium
Short Contributions
Keck Geology Consortium
Volume 38
May 2026
doi: 10.18277/AKRSG.2026.38.05

INVESTIGATING VOLCANICALLY FORCED SHIFTS IN NORTH PACIFIC CLIMATE IN MODEL SIMULATIONS AND ALASKA TREE RING RECORDS

LEV SUGERMAN-BROZAN, Colorado College
Project Advisors: Allison Lawman

INTRODUCTION

Volcanic eruptions can have long-lasting effects on climate. Eruptions inject sulfate aerosols into the atmosphere, reducing incoming shortwave radiation to the ocean-atmosphere system. This often has a large-scale cooling effect on the global ocean-atmosphere system (Cole-Dai, 2010). However, recent work has shown that volcanic eruptions can also have longer-lasting effects on key aspects of ocean-atmosphere circulation (e.g., Pausata et al., 2015; McGregor et al., 2020). For example, modelling has suggested that shifts in the Pacific Decadal Oscillation (PDO) include volcanically triggered 50-70-year PDO cycles (Sun et al., 2022). Despite an abundance of recent research on persisting climatic responses to volcanic forcings, the response of North Pacific climate variability remains unclear.

Here we use the Community Earth System Model Last Millenium Ensemble (CESM-LME, Otto-Bliesner et al., 2016) and a selection of mountain hemlock tree-ring chronologies from Alaska to investigate the North Pacific temperature and hydroclimate responses to volcanic forcing. A reconstruction based on the mountain hemlock chronologies show regional temperature changes following volcanic eruptions in 1258, 1452, 1697-1698 and 1809 CE.

We then use superposed epoch analysis to investigate the magnitude and duration of both the proxy-inferred and simulated surface temperature responses at the sites of the tree-ring chronologies during known volcanic events. This comparison helps identify both similarities and discrepancies between the model and data, therefore providing insights into the response of North Pacific climate to volcanic forcings. These findings will provide much-needed context for better understanding current and future changes in the North Pacific ocean-atmosphere system, and its response to external climate forcings.

BACKGROUND

The North Pacific is a region influenced by high internal variability, driven by the Pacific Decadal Oscillation (PDO), a long-lived El Niño Southern Oscillation (ENSO)-like pattern of ocean-atmosphere variability. The PDO is linked to North American climate variability, and typically occurs on 10-30 year cycles. Similar to ENSO, end-member phases of the PDO are characterized by anomalous sea surface temperatures (SSTs) and sea level pressure (SLP) in the North Pacific. The PDO also drives variability of the Aleutian Low (AL), a semipermanent low-pressure system in the Gulf of Alaska. The multiple overlapping modes of internal variability in the North Pacific is often difficult to disentangle from responses to volcanic forcings, making proxy records and multi-ensemble modeled datasets crucial for robust analysis.

The use of tree rings as climatic, ecological, hydrologic, and cultural proxies, called dendrochronology, has been a popular scientific method since the early twentieth century (e.g., Douglass, 1914). Tree rings have been found to be sensitive to a number of important climatic phenomena, including winter and summer temperatures, hydroclimate, and winter storminess (Wiles et al., 2014; Wilson et al., 2016; Gaglioti, 2019). Trees at high latitudes, such as those in the North Pacific, are primarily temperature-limited, and therefore are excellent proxies for growing season temperatures (e.g., Raspopov, 2004; Wiles et al., 2014) and associated internal climate variability (D'Arrigo et al., 2001; Davi et al., 2003). Dendrochronology also allows for annual resolution through cross-dating, the process of cross-referencing chronologies to obtain exact calendar year dates (Douglass, 1941). This process allows for exact correlation of chronologies to abrupt, year-scale temperature anomalies (e.g., volcanic eruption dates), making dendrochronological proxies an important record of volcanically-forced shifts in climate.

A mountain hemlock chronology from Wiles et al. (2014) reconstructs surface air temperature in the Gulf of Alaska (GOA) for the past 1200 years. The reconstruction displays internal variability on interannual and centennial timescales, suggested to correspond to solar/lunar tidal forcings and solar variability, respectively. The reconstruction also demonstrates prolonged cooling signals that correspond to multiple major volcanic events. These suggest not only well-documented externally-forced cooling signals, but also potentially coupled ocean-atmosphere responses to such forcings. The coastal location of the GOA temperature reconstruction suggests this proxy record may be sensitive to more prolonged, ocean-atmosphere coupled shifts in response to external forcings.

Though proxy-inferred responses are valuable records of climatic responses to external forcings, they often contain unwanted noise or internal variability. Multi-ensemble modeled datasets, such as the Community Earth System Model Last Millennium Ensemble (CESM-LME) allow for the reduction of such internal variability through multiple model runs (Otto-Bliesner et al., 2016). Each ensemble member begins with slightly different starting conditions, designed to replicate internal variability on both short and long timescales. The combination of such ensemble members (thirteen for the CESM-LME) allows for the approximate removal of internal variability; the ensemble mean thus isolates the forced signal. This effectively separates internal variability from the volcanically-forced cooling signal. Superposed epoch analysis (SEA) is a technique that isolates the specific time-window of an external forcing, aligning multiple events and separating coherent signals from noisier climate records.

Model-proxy comparisons are therefore powerful tools to test whether modeled mechanisms replicate real-world (e.g., proxy-inferred) responses to volcanic forcings. Though proxy records and climate models are inherently related (the CESM-LME uses forcing reconstructions based on proxy records; see Gao et al. (2008)), the comparison of controlled models (i.e., the removal of internal variability and isolation of external forcings) to the real-world proxy response often reveals valuable agreements or discrepancies. Proxy-model agreement can confirm proxy-inferred responses to volcanic eruptions and validate model accuracy, while discrepancies reveal limitations of proxy records or shortcomings of climate models. Proxy-model comparisons are therefore an effective methodology for evaluating proxy-inferred responses to external forcings.

METHODS

We performed a superposed epoch analysis (SEA) using growing season (January-September) surface air temperature reconstructed from tree rings (Wiles et al., 2014) and 2-meter air temperature modeled by the full-forcing member of the Community Earth System Model Last Millennium Ensemble (CESM-LME, Otto-Bliesner et al., 2016). We focus on the Gulf of Alaska (GOA) region, here subset to 50-60°N, 130-170°W (see Figure 1). The eruption events were selected for magnitude (as inferred from ice cores in Gao et al., 2008), well-constrained eruption dates, and existing literature (Gao et al., 2008; Leland et al., 2023). Here we use the 1258, 1452, 1697-1698, and 1809 events to facilitate comparison across the proxy record and the model.

The CESM-LME 2-meter air temperature data is subset to January-September. Area-weighted spatial means were calculated over the GOA region to ensure comparability with the entire proxy record. The time series are annually averaged for each growing season (Jan-Sep) and all thirteen ensemble members are averaged to reduce internal variability. The surface air temperature chronology, inferred from mountain hemlock trees in the GOA, was calculated by Wiles

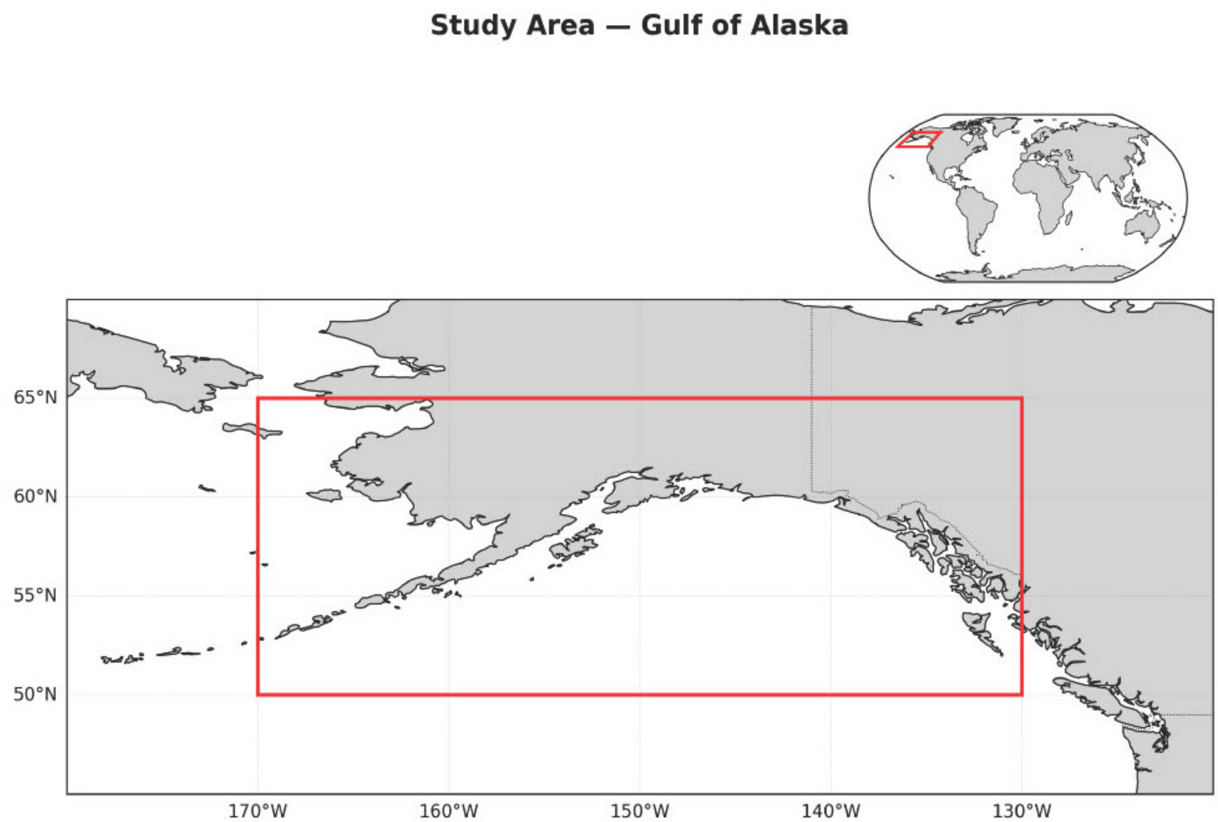

Figure 1. The study site in the Gulf of Alaska (GOA), 50°-60° N and 130°-170° W.

et al. (2014) according to their methods section. Mountain hemlock trees are sensitive to growing season temperature; the chronology therefore reflects January-September temperatures.

The SEA analysis aligned the time series for both the tree-ring chronology and the CESM-LME around the eruption year (e.g., Year 0), and extended Year -5 to Year +10 relative to each eruption. We calculated absolute temperature anomalies (°C) for ten years post-eruption compared to a five-year pre-eruption baseline. For the CESM-LME, the ensemble mean was calculated and compared to the thirteen individual ensemble members (Figure 2). Spatial, year-by-year anomalies were then calculated for the model data and displayed for the 1809 eruption (Figure 3) to investigate spatial cooling trends. Methodological consistency across the proxy record and model simulations allows for the investigation of post-eruption cooling magnitude, duration and spatial coherence, as well as proxy-model agreement or discrepancy.

RESULTS

Both the CESM-LME and the tree-ring chronology display cooling signals following major eruptions (1258, 1452, 1697-1698, 1809) compared to a five-year pre-eruption baseline. The modeled cooling response reaches a maximum of 1.7°C. The CESM-LME approaches pre-eruption baselines between 4 and 7 years post-eruption, and models spatially coherent cooling signals within the GOA (Figure 3). The magnitude of the cooling signal varies considerably across ensemble members. In contrast, the proxy-inferred cooling response has a higher maximum than the modeled at 2°C, and persists for between 5 and 8 years post-eruption.

The timing and the sign of the modeled and proxy-inferred post-eruption responses are therefore in agreement. However, there are significant discrepancies in the duration, amplitude, and variability of cooling signals between the modeled and proxy-inferred responses. The mechanisms for such discrepancies will be discussed in the following section.

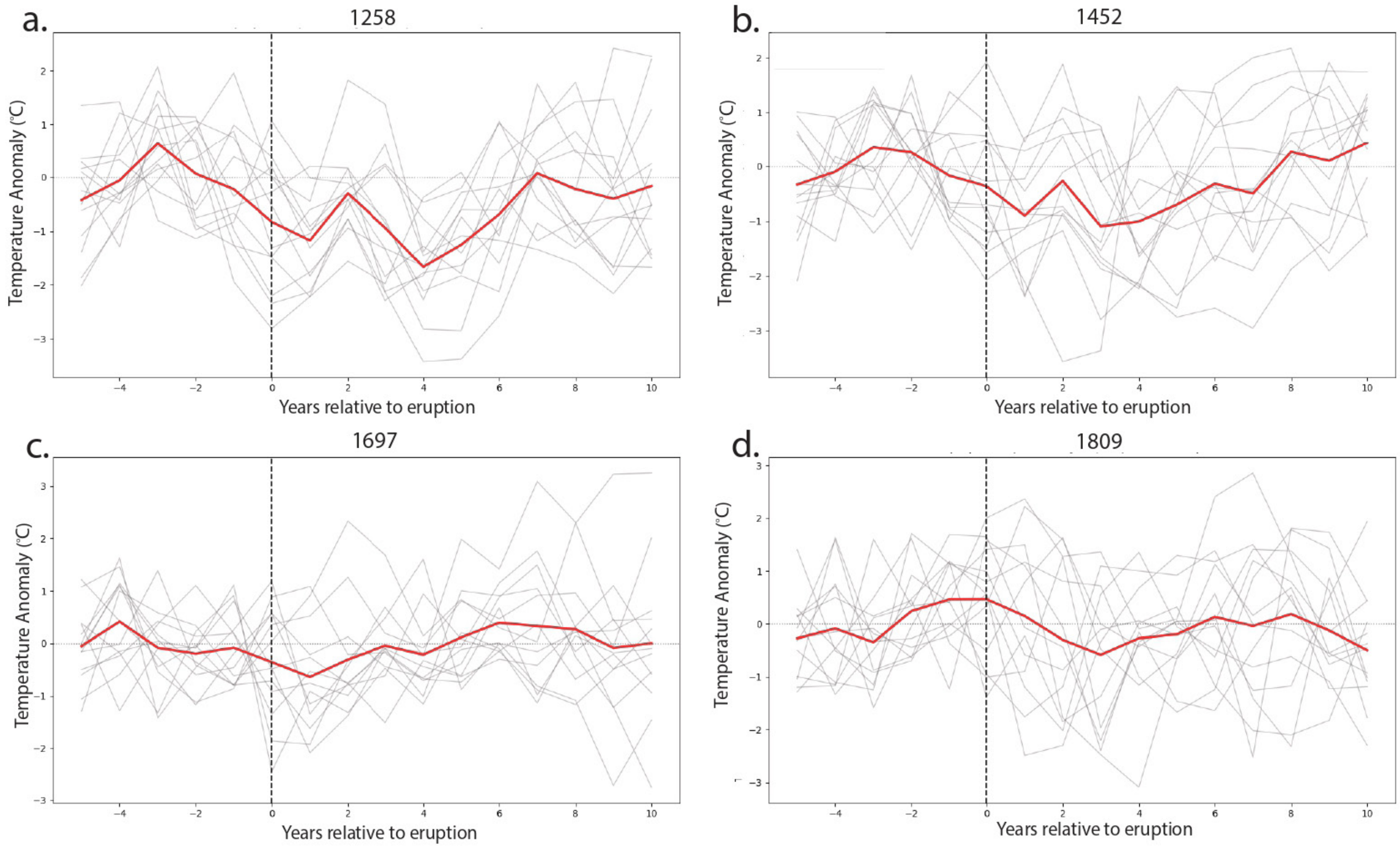

Figure 2. Superposed epoch analysis (SEA) for the 1258, 1452, 1697 and 1809 eruptions in the CESM-LME. Gray lines show the 13 individual ensemble members. The bolded red line shows the ensemble mean. Post-volcanic temperature changes are calculated relative to the 5-year pre-eruption baseline.

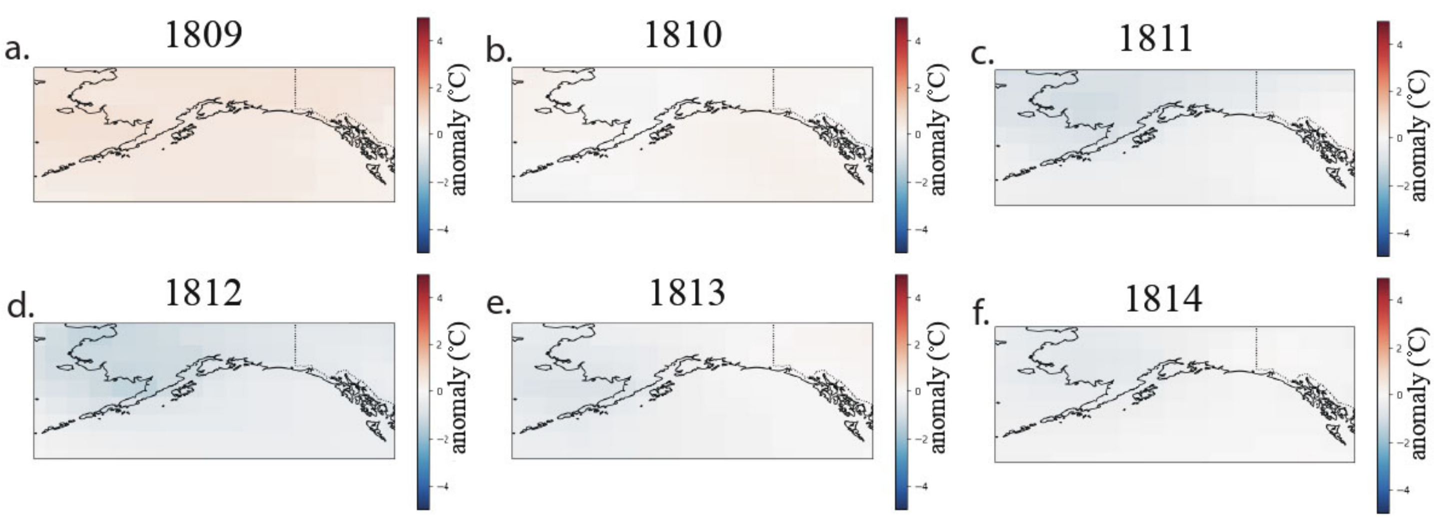

Figure 3. Spatial cooling trends in the GOA following the 1809 "mystery" eruption, as simulated in the 13 ensemble members of the full-forcing CESM-LME. Anomalies are calculated compared to the five-year pre-eruption baseline.

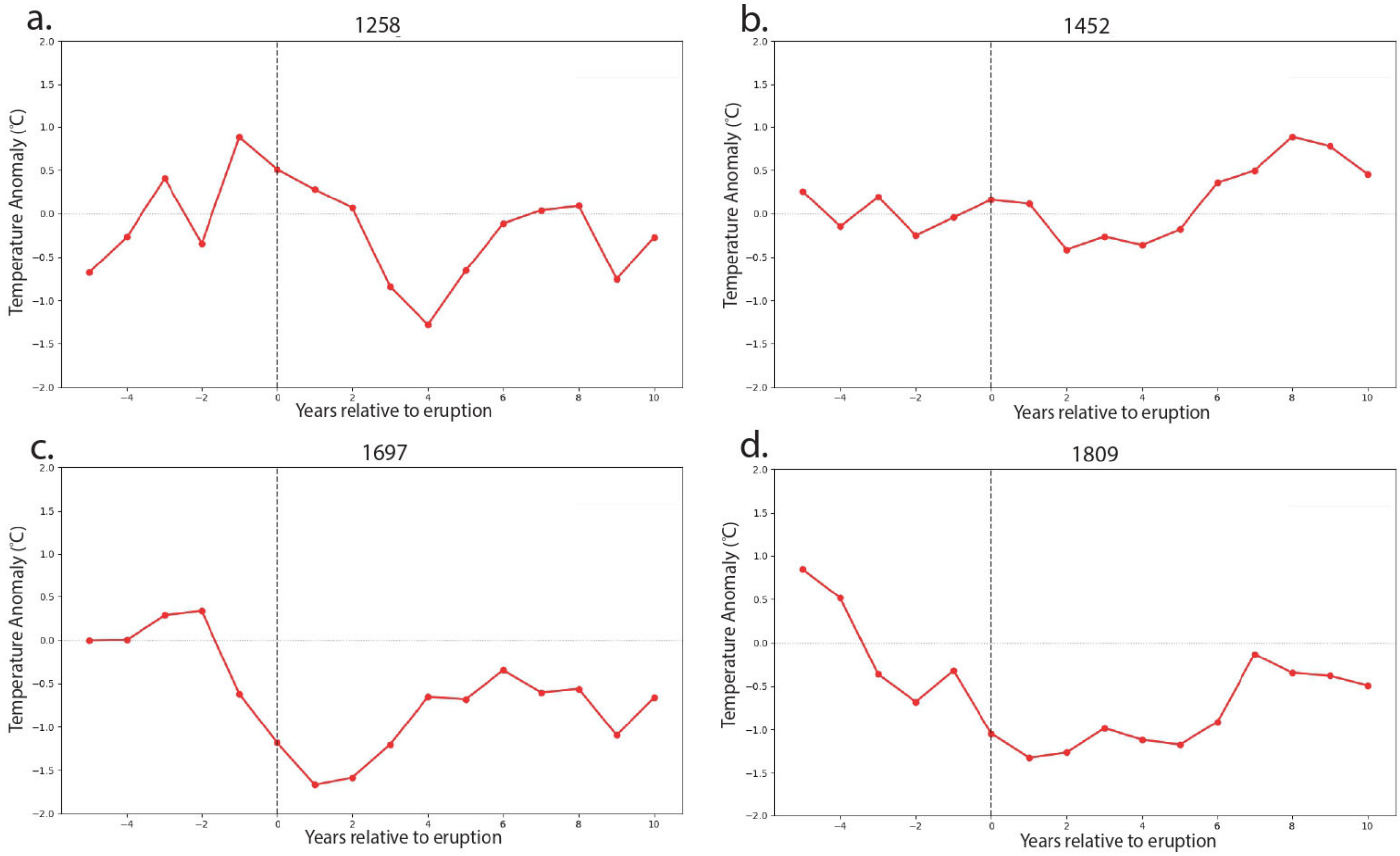

Figure 4. SEA for the Alaskan mountain hemlock temperature reconstruction for the same eruptions in Figure 2. Post-volcanic temperature changes are calculated relative to the 5-year pre-eruption baseline.

DISCUSSION

Our results replicate previous studies that show near-global cooling signals in response to large volcanic events (e.g., Cole-Dai, 2010). However, the considerable variability between ensemble members (Figure 2) in the modeled cooling response suggests that interannual variability plays a key role in modulating responses to external forcings in the North Pacific. Such variability may reflect ENSO or PDO phase, and therefore exerts controls on the magnitude, duration, and amplitude of forced responses to volcanic eruptions. The proxy-inferred cooling signals reflect the combined effects of forced responses and regional ocean-atmosphere circulation shifts. That these signals are longer-lasting and higher in magnitude (Figure 4) indicates the possible enhancement or dampening of forced signals by ocean-atmosphere coupled circulations and internal variability.

Specifically, the observed climatic response is dependent on the phase of climatic oscillations pre-eruption (Predybaylo et al., 2017), but more work is needed to determine the specific effects of pre-eruption phase on post-eruption responses. Volcanically-forced shifts in PDO phase have been proposed in previous work (Sun et al., 2022), as well as shifts in ENSO variability and magnitude (McGregor et al., 2020; Pausata et al., 2020), yet the exact effects on climatic oscillations similarly remain unclear. Such changes could feasibly produce changes in global teleconnections (Zhang et al., 2025), leading to truly global climatic changes. Post-volcanic cooling also alters the ocean's heat budget, mixed layer depth, and mixing capacity (Church et al., 2005), which exerts controls on the persistence and recovery time of post-eruption cooling. The discrepancies between ensemble members, as well as between the proxies and the model, show that these complex ocean-atmosphere interactions mask post-eruption temperature signals, highlighting the need for further work on responses of such interactions in the North Pacific to external forcings to better understand the mechanisms behind volcanically-forced shifts in climate.

Though the proxy-inferred cooling signals are sensitive to both external forcings (e.g., volcanic eruptions) and internal variability, they are also sensitive to a number of other non-climatic factors, including biological and ecological influences on growth, seasonal bias (January-September), and other local dynamics. These factors, similar to internal variability, can amplify or dampen forced signals. As such, caution must be exercised when utilizing proxy-inferred responses to volcanic forcings. Climate models have similar limitations in evaluating volcanic cooling signals, namely that many existing models, including the CESM-LME, often underestimate certain modes of internal variability. The CESM-LME may also not fully capture regional dynamics and ocean-atmosphere coupled interactions due to its relatively coarse resolution (1.9° x 2.5°).

Despite these limitations, our results demonstrate modeled and proxy-inferred post-volcanic cooling signals in the GOA. There is proxy-model agreement on the timing and sign of such responses. However, our results identify discrepancies between proxy data, model data and ensemble members, revealing that interannual ocean-atmosphere variability exerts key controls over the persistence and magnitude of volcanically forced shifts in climate. Understanding the specific mechanisms of such controls will aid in the interpretation of both past and future regional climate shifts in response to external forcing.

CONCLUSIONS

We found spatially coherent, persistent cooling signals in both the proxy-inferred and modeled responses to major volcanic eruptions in the Gulf of Alaska, as well as important discrepancies in the persistence and magnitude of such signals. Based on these results, we draw the following conclusions:

- Proxy and model data support a post-volcanic cooling signal in the Gulf of Alaska in response to major volcanic eruptions.

- Ocean-atmosphere coupled oscillations modulate the persistence and magnitude of the climatic response to such forcings.

Further work will investigate interannual to decadal changes as well as potential ocean-atmosphere oscillation phase shifts in response to volcanic forcings.

ACKNOWLEDGEMENTS

This material is based upon work supported by the Keck Geology Consortium and the National Science Foundation under Grant No. 2050697. Funding was provided to this project by a 2025-2026 Keck Geology Consortium Advanced Research Grant. We would like to thank Alaska Youth Stewards for their indispensable help in collecting samples.

REFERENCES

Brad Adams, J., Mann, M. E., & Ammann, C. M. (2003). Proxy evidence for an El Niño-like response to volcanic forcing. Nature, 426(6964), 274-278.

Church, J. A., White, N. J., & Arblaster, J. M. (2005). Significant decadal-scale impact of volcanic eruptions on sea level and ocean heat content. Nature, 438(7064), 74-77.

Cole-Dai, J. (2010). Volcanoes and climate. Wiley Interdisciplinary Reviews: Climate Change, 1(6), 824-839.

D'Arrigo, R., Villalba, R., & Wiles, G. (2001). Tree-ring estimates of Pacific decadal climate variability. Climate Dynamics, 18(3), 219-224.

Davi, N. K., Jacoby, G. C., & Wiles, G. C. (2003). Boreal temperature variability inferred from maximum latewood density and tree-ring width data, Wrangell Mountain region, Alaska. Quaternary Research, 60(3), 252-262.

Dee, S. G., Cobb, K. M., Emile-Geay, J., Ault, T. R., Edwards, R. L., Cheng, H., & Charles, C. D. (2020). No consistent ENSO response to volcanic forcing over the last millennium. Science, 367(6485), 1477-1481.

Douglass, A. E. (1914). A method of estimating rainfall by the growth of trees. Bulletin of the American Geographical Society, 46(5), 321-335.

Douglass, A. E. (1941). Crossdating in dendrochronology. Journal of Forestry, 39(10), 825-831.

Gaglioti, B. V., Mann, D. H., Williams, A. P., Wiles, G. C., Stoffel, M., Oelkers, R., ... & Andreu-Hayles,

L. (2019). Traumatic resin ducts in Alaska mountain hemlock trees provide a new proxy for winter storminess. Journal of Geophysical Research: Biogeosciences, 124(7), 1923-1938.

Gao, C., Robock, A., & Ammann, C. (2008). Volcanic forcing of climate over the past 1500 years: An improved ice core-based index for climate models. Journal of Geophysical Research: Atmospheres, 113(D23).

Latif, M., & Barnett, T. P. (1996). Decadal climate variability over the North Pacific and North America: Dynamics and predictability. Journal of Climate, 9(10), 2407-2423.

Leland, C. et al., 2023, A Spatiotemporal Assessment of Extreme Cold in Northwestern North America Following the Unidentified 1809 CE Volcanic Eruption: Paleoceanography and Paleoclimatology, v. 38, p. e2022PA004581, doi:10.1029/2022PA004581.

McGregor, S., Khodri, M., Maher, N., Ohba, M., Pausata, F. S., & Stevenson, S. (2020). The effect of strong volcanic eruptions on ENSO. El Niño Southern Oscillation in a changing climate, 267-287.

Nakamura, H., Lin, G., & Yamagata, T. (1997). Decadal climate variability in the North Pacific during the recent decades. Bulletin of the American Meteorological Society, 78(10), 2215-2226.

Otto-Bliesner, B. L., Brady, E. C., Fasullo, J., Jahn, A., Landrum, L., Stevenson, S., ... & Strand, G. (2016). Climate variability and change since 850 CE: An ensemble approach with the Community Earth System Model. Bulletin of the American Meteorological Society, 97(5), 735-754.

Pausata, F. S., Chafik, L., Caballero, R., & Battisti, D. S. (2015). Impacts of high-latitude volcanic eruptions on ENSO and AMOC. Proceedings of the National Academy of Sciences, 112(45), 13784-13788.

Pausata, F. S., Zanchettin, D., Karamperidou, C., Caballero, R., & Battisti, D. S. (2020). ITCZ shift and extratropical teleconnections drive ENSO response to volcanic eruptions. Science Advances, 6(23), eaaz5006.

Predybaylo, E., Stenchikov, G. L., Wittenberg, A. T., & Zeng, F. (2017). Impacts of a Pinatubo-size volcanic eruption on ENSO. Journal of Geophysical Research: Atmospheres, 122(2), 925-947.

Raspopov, O. M., Dergachev, V. A., & Kolström, T. (2004). Periodicity of climate conditions and solar variability derived from dendrochronological and other palaeoclimatic data in high latitudes. Palaeogeography, Palaeoclimatology, Palaeoecology, 209(1-4), 127-139.

Sun, W., Liu, J., Wang, B., Chen, D., & Gao, C. (2022). Pacific multidecadal (50–70 year) variability instigated by volcanic forcing during the Little Ice Age (1250–1850). Climate dynamics, 59(1), 231-244.

Wang, T., Otterå, O. H., Gao, Y., & Wang, H. (2012). The response of the North Pacific Decadal Variability to strong tropical volcanic eruptions. Climate Dynamics, 39(12), 2917-2936.

Wiles, G. C., D'Arrigo, R. D., Barclay, D., Wilson, R. S., Jarvis, S. K., Vargo, L., & Frank, D. (2014). Surface air temperature variability reconstructed with tree rings for the Gulf of Alaska over the past 1200 years. The Holocene, 24(2), 198-208.

Wilson, R., Anchukaitis, K., Briffa, K. R., Büntgen, U., Cook, E., D'Arrigo, R., ... & Zorita, E. (2016). Last millennium northern hemisphere summer temperatures from tree rings: Part I: The long term context. Quaternary Science Reviews, 134, 1-18.

Wu, C. H., Lee, S. Y., Tsai, I. C., Shiu, C. J., & Chen, Y. Y. (2023). Volcanic contribution to the 1990s North Pacific climate shift in winter. Scientific Reports, 13(1), 5672.

Zhang, X., Li, J., Xie, S. P., Liu, F., Shi, F., Gao, C., ... & Dong, Q. (2025). Volcanic eruptions disrupt ENSO teleconnections with land summer temperature. Nature Communications, 16(1), 9882.

KECK Geology Consortium
Learning Science Through Research
Published by the Keck Geology Consortium
Short Contributions
Keck Geology Consortium
Volume 38
May 2026
doi: 10.18277/AKRSG.2026.38.06

SEVENTEENTH CENTURY VOLCANIC-INDUCED COOLING SIGNALED BY TREE RING GROWTH, GULF OF ALASKA

LANDON VAUGHAN, Trinity University
Project Advisor: Benjamin Surpless

ABSTRACT

Oral histories from the Huna Tlingit of southeast Alaska chronicle an interval of extreme cold, when winter succeeded the previous winter without an intervening summer. At this time, the advance of the Sit'Tlein glacier forced the Huna Tlingit to emigrate from their homeland, in Glacier Bay, further southward. The timing of this protracted winter is uncertain. Recent work in Scotland links 17th-century volcanism to an extreme cooling event in the mid-to-high latitudes, and the coldest summers identified in multiple northwest European tree-ring series are 1698, 1699, and 1700. Seventeenth-century volcanism is likely the cause of the cold period documented along 55-60 N latitude in Europe. A similar marker has been identified, though not yet studied, in the North Pacific sector. We analyze tree ring data from Yellow Cedar (YC) and Mountain Hemlock (MH), two temperature sensitive tree species in Southeast Alaska, to provide insight into temperatures from 1550 to 1850 CE. We selected 13 total locations from the International Tree Ring Data Bank (ITRDB) with a combined sample size of approximately 300 trees during the 300-year window of interest. Trends in MH and YC ring thicknesses correlate strongly with the volcanic-induced cooling event previously documented in Scotland. Though 1698-99 is a strong candidate for the "winter following winter" documented in oral histories, it's possible that the longer period of cold we document in this study was responsible for the rapid advance of the Sit'Tlein glacier and the resulting migration of the Huna Tlingit people.

INTRODUCTION AND BACKGROUND

The focus of this study is to characterize a cooling event in the Gulf of Alaska during the late 1600s in a global context. This cooling event is well-established in other high-latitude regions, but it has only recently been identified in the Gulf of Alaska (GOA) based on summer temperature-sensitive tree ring chronologies, including Mountain Hemlock (Wiles et al., 2014). Several large volcanic eruptions (perhaps six) occurred throughout the 1600s, all of which were climatically effective; their release of gas and aerosols caused brief or even long-term climate changes (Briffa et. al., 1998). Briffa et al. (1998) used climate-proxy ice core data to date significant eruptions in the years 1601, 1641-43, 1659, 1675, 1695, and 1698/9. We focus on the 1690s eruptions, which fall within an interval of extreme cold documented in Scotland (D'Arrigo et. al., 2020).

D'Arrigo et al., (2020) attribute extreme cooling of Scotland and northwestern Europe during the late 1690s and early 1700s to volcanic-induced climate change. The coldest summers in multiple tree-ring series are 1698, 1699, and/or 1700, which correspond to the Seven Ill Years, a period of famine and economic hardship in Scotland (D'Arrigo et al., 2020). D'Arrigo et al., (2020) reconstructed Scottish mainland summer temperatures from 1200 to 2000 CE and demonstrated that the coldest decade during this period was the 1690s (Fig. 1). D'Arrigo et al. (2020) used historical datasets from the British Isles and northern Europe to corroborate Scottish data and established that the 1690s cooling was hemisphere-scale. D'Arrigo et al. (2020) suggest that the cause of

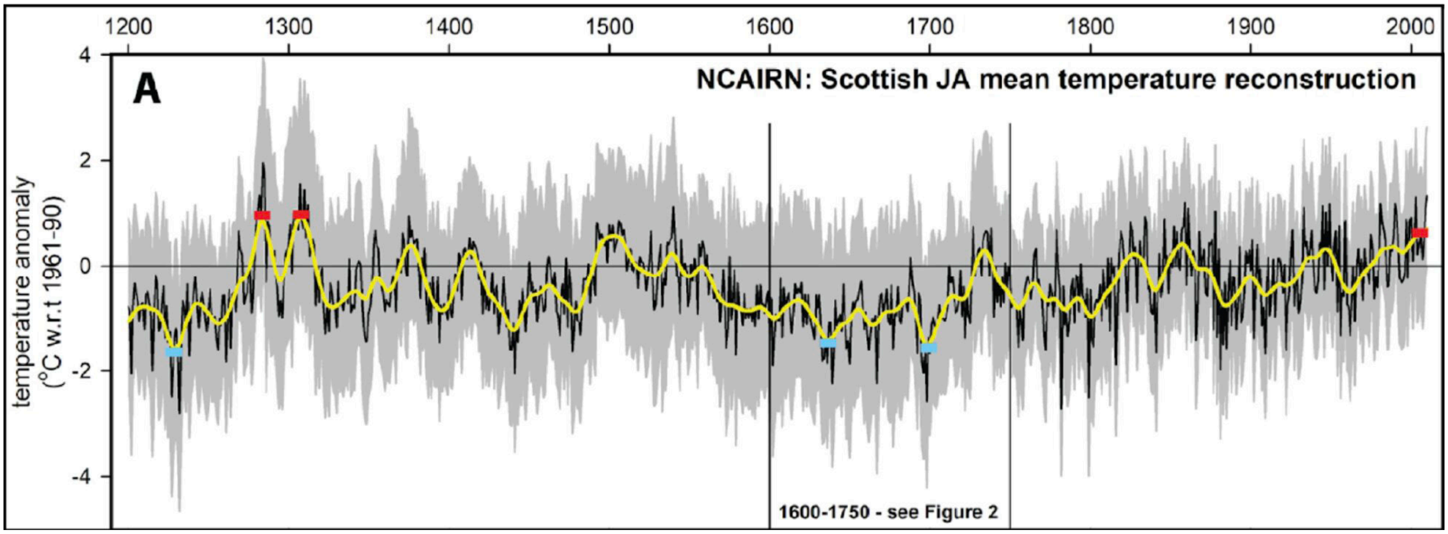

Figure 1. Scottish mainland summer (July-August) temperature reconstruction (D'Arrigo et al., 2020). The coldest decades, including the 1690s, are indicated by blue squares while the warmest are indicated by red squares. The yellow line represents a running average of the data.

this period of cold was a period of active volcanism in the seventeenth century.

The 1690s cold interval occurred during the Little Ice Age (LIA) (Crowley et al., 2008; Sun et al., 2022). Miller et al. (2012) postulate that cooling in the LIA was, in part, triggered by phases of frequent volcanism beginning around 1250 CE and intensifying around 1600 CE. The Maunder Minimum, a period of extremely low solar activity, also coincides with this period, amplifying cold temperature anomalies during the 1645-1715 interval (Bourgeois, 2015). The advance of glaciers in the Arctic and subarctic was a direct consequence of these feedback systems (Luckman, 2000). Lawson et al (unpublished) reconstructed the advance of the Tidewater (Sit' Tlein) glacier in southeast Alaska based on tree ring data. The rapid advance of the Sit' Tlein glacier coincides with the beginning of the eighteenth century, a result of the prevailing anomalously cold temperatures.

Leland et al. (2023) conducted a similar study in Alaska and established two climatically effective volcanic eruptions during the early 1800s that were responsible for another of the Little Ice Age's coldest intervals (Leland et al., 2023). A low-latitude, tropical eruption in 1809 triggered intense cooling in the Gulf of Alaska, identified through tree-ring proxy data (Leland et al., 2023). These studies along the Gulf of Alaska, based primarily on tree-ring-based temperature reconstructions, have demonstrated similar timing to cooling periods established at Scotland, also at high-latitude (e.g., Leland et al., 2023).

Lastly, oral histories from the Huna Tlingit of southeast Alaska chronicle an interval of extreme cold in their homeland, where winter abruptly succeeded the previous winter without an intervening summer (Hinkley et al., 2026). Huna Tlingit people "began to be in want of food," and shortly before or at this time, they were forced off their homeland in Glacier Bay due to the advancing Sit'Tlein glacier (Swanton, 1909). However, the precise timing of this protracted winter has only been speculated. The hunter-gatherer lifestyle of Alaska's coastal indigenous communities has long been threatened by climate change—particularly cooling periods that alter sea surface temperatures, disrupting both marine and terrestrial food sources (Crowell et al., 2023).

METHODS

We selected seven Yellow Cedar (YC) and six Mountain Hemlock (MH) locations for analysis from the International Tree Ring Data Bank (ITRDB; Fig. 2). We limited our analysis to data that included ring widths covering the entire interval of interest (1550 - 1850 CE) and at latitudes similar to northwestern Europe (between 55°N and 60°N). We focused on the interval from 1550 to 1850 CE for our analyses. Those not already standardized were first compiled in COFECHA (Holmes, 1983), a dendrochronology software program that crossdates tree-ring data serves as a quality control on tree-ring dating. The resulting COFECHA master chronologies retain their high frequency (year to year) variability and were used in subsequent analyses.

For each species, we combined ring width indices, by averaging the multiple ring-width series into one mean ring width index (RWI) for each year. With these data, we then smoothed chronologies for each species with a fifteen-year running average to eliminate small-scale variability. We correlated each chronology with mean summer (Jun-Aug) temperature data from Juneau, AK, in KNMI Climate Explorer (Trouet et al., 2013). Afterwards, we averaged the two species-specific chronologies to create a master temperature-sensitive chronology representative of the entire study area (Fig. 2). Finally, we applied 10-year running averages to each species-specific chronology to capture decadal variability.

RESULTS AND DISCUSSION

Tree ring data from the thirteen stands of temperature-sensitive tree species reveal similar ring width trends in response to shifting climate conditions through time (Fig. 3). Each species chronology shows similar fluctuations in ring width thicknesses during the period from 1550 to 1850 CE. Notable cold pulses are recorded by both species, including a pulse that occurs around the year 1700 CE (Fig. 3).

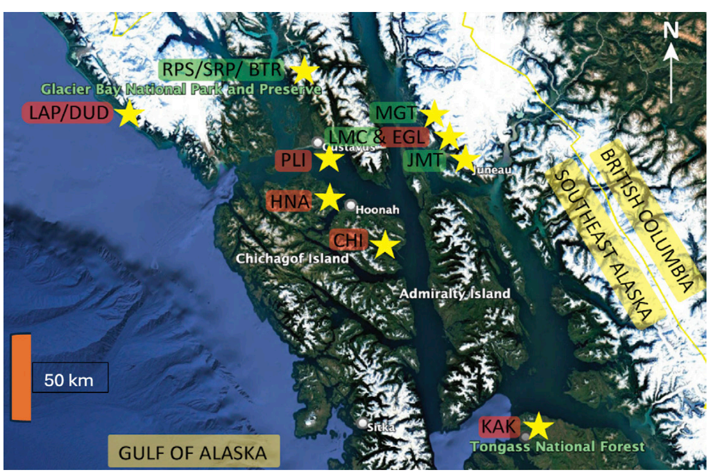

Figure 2. Locations of each tree ring chronology used for this study. Locations (yellow stars) are labeled with a three-letter abbreviation. Red shading represents Yellow Cedar stands, and green Mountain Hemlock sites. We obtained all data from the ITRDB.

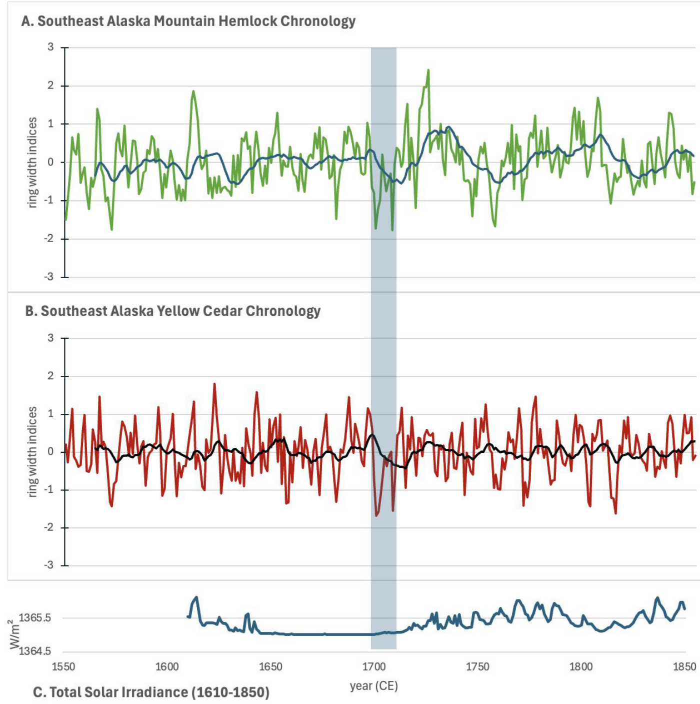

Figure 3. A. Averaged ring-width data from six Mountain Hemlock locations. Values above or below y=0 represent thicker or thinner than average ring widths, respectively. Blue line shows the 15-year rolling average of the data. B. Averaged ring-width data from seven Yellow Cedar locations. Values above or below y=0 represent thicker or thinner than average ring widths, respectively. Black line shows 15-year rolling average of the data. C. Reconstructed total solar irradiance reveals the presence of a Maunder Minimum from 1645-1715 (Lean et al., 1995) during the ongoing Little Ice Age. The period of intense cooling from 1695 to 1708 is shaded in blue.

The decadal moving averages reduce noise and small-scale variability, to each species-specific chronology (Fig. 4) and together the Mountain Hemlock (green line) and Yellow Cedar (red line) chronologies show consistency, especially relative to previously established regional and global (Fig. 1) cold pulses occurring around 1700 and 1810 CE. The ~1810 cooling is associated with a recently analyzed volcanic eruption and subsequent cooling (Leland et al., 2023). The ~1700 CE cooling event documented in the Gulf of Alaska correlates well with northwest European Summer Temperature reconstructions (Fig. 1) (D'Arrigo et al., 2020).

For the Mountain Hemlock species, the coldest year from 1550 to 1850 CE is 1706 (Table 1). For the Yellow Cedar species, the coldest year is 1698 (Table 1). The coldest decade for both species is 1697-1706. For the combined data, the coldest year in the Gulf of Alaska is 1698, and the coldest decade

Table 1. Ranked annual and decadal ring-width temperature proxy data.

	Mountain Hemlock		Yellow Cedar		Combined	
Rank	Annual	Decadal	Annual	Decadal	Annual	Decadal
1	1706	1697 - 1706	1698	1697 - 1706	1698	1697 - 1706
2	1572	1698 - 1707	1812	1698 - 1707	1706	1698 - 1707
3	1698	1696 - 1705	1699	1696 - 1705	1572	1696 - 1705
4	1755	1620 - 1629	1706	1696 - 1705	1699	1699 - 1708
5	1754	1618 - 1627	1572	1695 - 1704	1679	1695 - 1704
6	1550	1619 - 1628	1800	1624 - 1633	1571	1624 - 1633
7	1679	1695 - 1704	1768	1806 - 1815	1754	1751 - 1760
8	1571	1622 - 1631	1655	1567 - 1576	1768	1752 - 1761
9	1744	1751 - 1760	1571	1626 - 1635	1810	1567 - 1576
10	1699	1621 - 1630	1656	1752 - 1761	1755	1753 - 1762

Note: ranked from thinnest (low T) to thickest (high T) ring-widths.

is 1697-1706 (Table 1). The decadal rolling average on the combined data shows a pronounced period of prolonged cooling, from 1695 to 1708 (Fig. 4). Variability between the two species is sharply reduced during the 1690s cooling period, which correlates with the same period established in Northwestern Europe by D'Arrigo et al. (2020). In addition, an early 1800s cooling event displays a similar decrease in tree growth and corresponds well with the same cold period identified in the Gulf of Alaska by Leland et al. (2023).

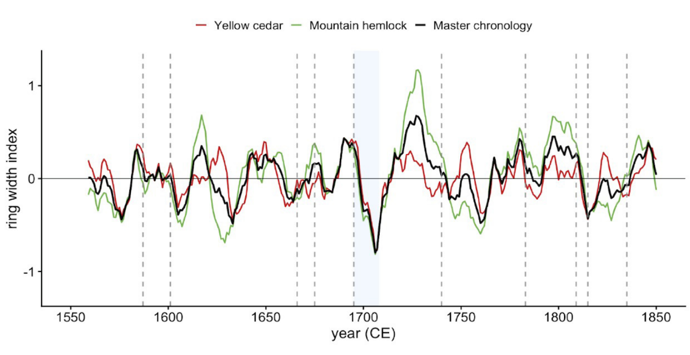

Figure 4. Decadal moving averages applied to Yellow Cedar (red line) and Mountain Hemlock (green line) species-specific chronologies. The black line represents the average of both species. A solid line at y = 0 represents the mean index. Vertical dashed lines represent climatically effective volcanic eruptions (Briffa et al., 1998). A period from 1695-1708 is shaded in pale blue, indicating the period of record cooling following the 1695 volcanic eruption with unknown origin, corresponding to table values (Table 1).

CONCLUSION

Yellow Cedar and Mountain Hemlock tree-ring-based summer temperature reconstructions in Southeast Alaska provide an improved understanding of volcanic activity's impact on regional temperature anomalies and climate extremes. The period of cold identified in Southeast Alaska during the 1690s and early 1700s reflects a similar duration and intensity to a previously identified event at similar latitudes in northwestern Europe. The consistency in data at both locations suggests that climatically effective eruptions in the late seventeenth century which prompted a period of intense cooling in the mid-to-high latitudes. The period of cold we document in this study had an impact on agriculture, socioeconomics, and human suffering, as recorded in the Seven Ill Years in Scotland. At the same time, unusual cold in Southeast Alaska may have forced human migration because of food insecurity and rapid glacial advance in Glacier Bay.

ACKNOWLEDGEMENTS

This material is based upon work supported by the KECK Geology Consortium and the National Science Foundation under Grant No. 2050697. I'd like to thank Dr. Greg Wiles and Nick Wiesenberg from the College of Wooster Tree Ring Lab in Ohio, as well as Dr. Ben Surpless of Trinity University. Additionally, I give gratitude to my summer (2025) research partners and the gracious people of Angoon, Admiralty Island, Alaska, who offered peerhood, mentorship, and friendship along the way.

REFERENCES

Bourgeois, C., et al. "Ice Age Trees in the Arctic." Astronomy & Astrophysics 583 (September 2015). https://www.aanda.org/articles/aa/full_html/2015/09/aa26652-15/aa26652-15.html.

Briffa, Keith R., Philip D. Jones, Fritz H. Schweingruber, and Timothy J. Osborn. 1998. "Influence of Volcanic Eruptions on Northern Hemisphere Summer Temperature over the Past 600 Years." Nature 393 (6684): 450–455. https://doi.org/10.1038/30943.

Crowell, Aron L., and Mayumi L. Arimitsu. 2023.

"Climate Change and Pulse Migration: Intermittent Chugach Inuit Occupation of Glacial Fiords on the Kenai Coast, Alaska." Frontiers in Environmental Archaeology 2 (1145220): 1–27. https://doi.org/10.3389/fearc.2023.114522.

Crowley, T. J., G. A. Zielinski, B. M. Vinther, R. Udisti, K. Kreutz, J. Cole-Dai, and E. Castellano. 2008. "Volcanism and the Little Ice Age." PAGES News 16 (2): 22–23. https://www.researchgate.net/publication/256476383_Volcanism_and_the_Little_Ice_Age.

D'Arrigo, Rosanne, Patrick Klinger, Timothy Newfield, Miloš Rydval, and Rob Wilson. 2020. "Complexity in Crisis: The Volcanic Cold Pulse of the 1690s and the Consequences of Scotland's Failure to Cope." Journal of Volcanology and Geothermal Research 389: 106746. https://www.sciencedirect.com/science/article/pii/S0377027319303087.

Hinkley, L.W., Cooper, T., Gaglioti, B., Navareaz, J., Wiesenberg, N. and Wiles, G.C., 2023, The intersection of oral histories and tree-ring chronologies in Southeast Alaska: Geological Society of America Abstracts with Programs. Vol. 55, No. 6, doi: 10.1130/abs/2023AM-392714

Holmes, R.L. (1983). "Computer-assisted quality control in tree-ring dating and measurement." Tree-Ring Bulletin, 43, 69–78.

Lawson, D., et al. Tidewater Glacier Fluctuations During the Last 2000 Years, Glacier Bay National Park and Preserve, Southeast Alaska, USA. Unpublished manuscript.

Leland, C., D'Arrigo, R., Davi, N., Anchukaitis, K.J., Andreu-Hayles, L., Porter, T.L., Galloway, T., Mant, M., Wiles, G., Wilson, R., Beaulieu, S., Oelkers, R., Gaglioti, B.V., Rao, M.P., Reid, E., Nixon, T., 2023, A Spatiotemporal Assessment of Extreme Cold in Northwestern North America Following the Unidentified 1809 CE Volcanic Eruption. Paleoceanography and Paleoclimatology 38 (5): e2022PA004581. https://doi.org/10.1029/2022PA004581.

Luckman, B.H., 2000, The Little Ice Age in the Canadian Rockies: Geomorphology, v. 32, no. 3–4, p. 357–384, https://doi.org/10.1016/S0169-555X(99)00104-X

Miller, G. H., et al. "Abrupt Onset of the Little Ice Age Triggered by Volcanism and Sustained by Sea-Ice/Ocean Feedbacks." Geophysical Research Letters 39, no. 2 (2012). https://doi.org/10.1029/2011GL050168.

NOAA Paleoclimatology Program. "Tree Ring." Accessed September 3, 2025. https://www.ncei.noaa.gov/products/paleoclimatology/tree-ring.

Sun, Weiyi, Jingyuan Liu, Bin Wang, Deliang Chen, and Chengcheng Gao. 2022. "Pacific Multidecadal (50–70 Year) Variability Instigated by Volcanic Forcing during the Little Ice Age (1250–1850)." Climate Dynamics 59: 231–244. https://doi.org/10.1007/s00382-021-06127-7.

Swanton, John R. 1909. Tlingit Myths and Texts. Bureau of American Ethnology Bulletin 39. Washington, DC: U.S. Government Printing Office.

Trouet, Valerie, and Geert Jan van Oldenborgh. "KNMI Climate Explorer: A Web-Based Research Tool for High-Resolution Paleoclimatology." Tree-Ring Research 69, no. 1 (2013): 3–13. https://doi.org/10.3959/1536-1098-69.1.3.

Wiles, G.C., D'Arrigo R.D., Barclay, D., Wilson, Jarvis, S.K., Vargo, L., Frank, D., 2014, Surface air temperature variability for the Gulf of Alaska over the past 1200 years: The Holocene, DOI: 10.1177/0959683613516815.